# Climatic impacts of vegetation dynamics in Eastern Africa

TEMESGEN ALEMAYEHU ABERA

ACADEMIC DISSERTATION
To be presented, with the permission of the Faculty of Science of
the University of Helsinki, for public examination in Auditorium A110 of
the Chemicum building of the University of Helsinki, on 6th March 2020, at 12 noon.

**DEPARTMENT OF GEOSCIENCES AND GEOGRAPHY A80** / HELSINKI 2020

Author's address: Temesgen Alemayehu Abera
Department of Geosciences and Geography
P.O. Box 64, FIN-00014 University of Helsinki, Finland
temesgen.abera@helsinki.fi

Supervisors: Professor Petri Pellikka
Department of Geosciences and Geography
University of Helsinki, Finland

Dr. Janne Heiskanen
Department of Geosciences and Geography
University of Helsinki, Finland

Dr. Eduardo Maeda
Department of Geosciences and Geography
University of Helsinki, Finland

Pre-examiners: Professor Jukka Käyhkö
Section of Geography, Department of Geography and Geology
University of Turku, Finland

Associate Professor Youngryel Ryu
Department of Landscape Architecture and Rural Systems Engineering
Seoul National University, Republic of Korea

Opponent: Professor Rasmus Fensholt
Department of Geosciences and Natural Resource Management
University of Copenhagen, Denmark

ISSN-L 1798-7911
ISSN 1798-7911 (print)
ISBN 978-951-51-4928-2 (paperback)
ISBN 978-951-51-4929-9 (PDF)
http://ethesis.helsinki.fi

Unigrafia Oy
Helsinki 2020

**Abera, T.A.,** (2020). Climatic impacts of vegetation dynamics in Eastern Africa. Department of Geosciences and Geography, University of Helsinki, A80. Unigrafia, Helsinki.

## Abstract

The climate system responds to changes in the structure and physiology of vegetation. These changes can be induced by seasonal growing cycles, anthropogenic land cover changes (LCCs), and precipitation extremes. The extent to which vegetation changes impact the climate depends on the type of ecosystem, the season, and the intensity of perturbations from LCCs and precipitation extremes. Under the growing impacts of climate change and human modification of natural vegetation cover, understanding and monitoring the underlying biogeophysical processes through which vegetation affects the climate are central to the development and implementation of effective land use plans and mitigation measures.

In Eastern Africa (EA) the vegetation is characterized by multiple growing cycles and affected by agricultural expansion as well as recurrent and severe drought events. Nonetheless, the degrees to which vegetation changes affect the surface energy budget and land surface temperature (LST) remain uncertain. Moreover, the relative contributions of various biogeophysical mechanisms to land surface warming or cooling across biomes, seasons, and scales (regional to local) are unknown. The objective of this thesis was to analyze and quantify the climatic impacts of land changes induced by vegetation seasonal dynamics, agricultural expansion, and precipitation extremes in EA. In particular, this thesis investigated these impacts across biomes and spatio-temporal scales. To address this objective, satellite observation and meteorological data were utilized along with empirical models, observation-based metrics, and statistical methods.

The results showed that rainfall–vegetation interaction had a strong impact on LST seasonality across ecoregions and rainfall modality patterns. Furthermore, seasonal LST dynamics were largely controlled by evapotranspiration (ET) changes that offset the albedo impact on the surface radiation balance. Forest loss disturbed the LST dynamics and increased local LST consistently and notably during dry seasons, whereas during the wet season its impact was limited because of strong rainfall–vegetation interaction. Moreover, drought events affected LST anomalies; however, the impact of droughts on temperature anomalies was highly regulated by vegetation greening.

In addition, the conversion of forest to cropland generated the highest net warming (1.3 K) compared with other conversion types (savanna, shrubland, grassland, and cropland). Warming from the reduction of ET and surface roughness was up to ~10 times stronger than the cooling effect from albedo increases (−0.12 K). Furthermore, large scale analysis revealed a comparable warming magnitude during bushland-to-cropland conversion associated with the dominant impact of latent heat (LE) flux reduction, which outweighed the albedo effect by up to ~5 times. A similar mechanism

dominated the surface feedback during precipitation extremes; where LE flux anomalies dominated the energy exchange causing the strongest LST anomaly in grassland, followed by savanna. By contrast, the impact was negligible in forest ecosystems.

In conclusion, the results of this thesis clarify the mechanics and magnitude of the impacts of vegetation dynamics on LST across biomes and seasons. These results are crucial for guiding land use planning and climate change mitigation efforts in EA. The methods and results of this thesis can assist in the development of ecosystem-based mitigation strategies that are tailored to EA biomes. Moreover, they can be used for assessing the performance of climate models and observation-based global scale studies that focus on the biogeophysical impacts of LCCs.

**Keywords:** LST seasonality; Land cover change; Bushland (Acacia-Commiphora); Biophysical effects; Precipitation extremes; Satellite observation.

# Acknowledgements

My PhD study was an exciting journey of learning and inspiration. As an Ethiopian, I am lucky to research on critical environmental problems and contribute to the ongoing research in Eastern Africa. I have learned many ways to explore satellite observation data to study the impacts of vegetation change on surface-atmosphere energy and water exchanges and land surface temperature. This journey, however, would not have been successful without the technical and emotional support from many people.

First, I would like to thank my supervisors: Professor Petri Pellikka, Dr. Janne Heiskanen, and Dr. Eduardo Maeda. They have contributed a lot in advising, technically guiding my researches, and shaping my thoughts in addressing scientific problems. I am very thankful to Prof. Petri Pellikka, for warmly accepting me as a student in the University of Helsinki and for extending continuous support, advice, and encouragement throughout my studies. Am very grateful for the opportunity to participate in a research project in East Africa (TAITASMART). I thank Eduardo, who often showed me the bright side and pushed me forward when I was stuck. I have learned a lot from him, both technically and socially. I thank Janne for being there for me. Your excellent critics improved my knowledge. I appreciate Professor Miina Rautiainen and Dr. Hari Adhikari for being co-authors and having good discussions. I would like to express my gratitude to Professor Rasmus Fensholt for serving as an opponent and Professor Jukka Käyhkö and Associate Professor Youngryel Ryu for being the pre-examiners of this dissertation and their constructive comments.

I am grateful to my doctoral program, GeoDoc, for helping my participation in the European Geoscience Union (EGU) conference in Austria, Vienna. I thank all staff members and PhD students in the Department of Geosciences and Geography, Institute for Atmospheric and Earth System Research (INAR), and ECHOLAB group for being a nice colleague. Specially I would like to thank Antti Autio and his families for being a good friend and neighbour, and my colleagues and friends: Edward Amara, Hari Adhikari, Dr. Jinxiu Liu, Dr. Rami Piiroinen, Zhipeng Tang, Matti Räsänen, Peifeng Su, Ruut Uusitalo, Sheila Wachiye, Yang Liu, Dr. Mika Siljander, Pekka Hurskainen, Dr. Tino Johansson, Dr. Andrew Rebeiro-Hargrave, Dr. Matheus Nunes, Dr. Yhasmin Mendes, James Mwamodenyi , Martha Munyao, and Veronica. My best friend Dr. Binyam Tesfaw is appreciated for his encouragement and introducing me to Petri. I thank all friends who helped me from abroad.

Finally, I am deeply indebted to my family members (Kebebush, Alemayehu, Bizunesh, Adanech, Mihret, Yeab, Nathan, and Bini) for your prayers, love, patience, and support. My three amazing sisters, hearing about your excellent progress spurs happiness in my heart during my studies. My late brothers (Gudeta and Zelalem), you are still alive in my heart and am forever grateful for your love and kindness. Special thank goes to my beloved fiancée, Daniela, whom I met during my studies. You have encouraged, inspired, and been there for me during my studies. Am very lucky and happy to have you by my side during this important phase of my life.

# Contents

## List of original publications

I **Abera, T. A.,** Heiskanen, J., Pellikka, P. K. E., Maeda, E. E. (2018). Rainfall-vegetation interaction regulates temperature anomalies during extreme dry events in the Horn of Africa. Global and Planetary Change, 167, 35–45. https://doi.org/10.1016/j.gloplacha.2018.05.002

II **Abera, T. A.,** Heiskanen, J., Pellikka, P. K. E., Rautiainen, M., Maeda, E.E. (2019). Clarifying the role of radiative mechanisms in the spatio-temporal changes of land surface temperature across the Horn of Africa. Remote Sensing of Environment, 221, 210–224. https://doi.org/10.1016/j.rse.2018.11.024

III **Abera, T. A.,** Heiskanen, J., Pellikka, P. K. E., Maeda, E. E. (2020). Impact of rainfall extremes on energy exchange and surface temperature anomalies across biomes in the Horn of Africa. Agricultural and Forest Meteorology, 280, 107779. https://doi.org/10.1016/j.agrformet.2019.107779

IV **Abera, T. A.,** Heiskanen, J., Pellikka, P. K. E., Adhikari, H., Maeda, E. E. Climatic impacts of bushland to cropland conversion in Eastern Africa (Submitted).

## Authors's contribution

| | I | II | III | IV |
|---|---|---|---|---|
| Original idea | TA, EM | TA, EM | TA, EM | TA, JH, PP |
| Methodology design | TA, EM | TA, EM | TA | TA |
| Data collection and pre-processing | TA | TA | TA | TA, HA |
| Analysis | TA | TA | TA | TA |
| Interpretation of the results | TA, JH, EM | TA, JH, EM | TA, JH, EM | TA, JH, EM |
| Manuscript writing | TA | TA | TA | TA |
| Comment and revision | JH, EM, PP | JH, EM, PP, MR | JH, EM, PP | JH, EM, PP, HA |

TA = Temesgen Abera; JH = Janne Heiskanen; PP = Petri Pellikka;

EM = Eduardo Maeda; HA = Hari Adhikari; MR= Miina Rautiainen

# Abbreviations

| | |
|---|---|
| BRDF | Bidirectional reflectance distribution function |
| CERES | Clouds and the Earth's Radiant Energy System |
| CM SAF | Climate Monitoring Satellite Application Facility |
| EA | Eastern Africa |
| EBAF | Energy Balanced and Filled |
| EBD | Energy balance decomposition |
| ENSO | El Niño–Southern Oscillation |
| ENVI | Environment for Visualizing Images |
| ET | Evapotranspiration |
| EUMETSAT | European Organisation for the Exploitation of Meteorological Satellites |
| EVI | Enhanced vegetation index |
| FAO | Food and Agriculture Organization |
| FLAASH | Fast Line-of-sight Atmospheric Analysis of Hypercubes |
| FLUXNET | Flux Network |
| GHG | Greenhouse gas |
| GLASS | Global Land Surface Satellite |
| GLEAM | Global Land Evaporation Amsterdam Model |
| GTOPO | Global digital elevation model |
| H | Sensible heat |
| HoA | Horn of Africa |
| IBPM | Intrinsic Biophysical Mechanism |
| IGBP | International Geosphere-Biosphere Programme |
| IOD | Indian Ocean Dipole |
| IPCC | Intergovernmental Panel on Climate Change |
| ITCZ | Intertropical Convergence Zone |
| JAXA | Japan Aerospace Exploration Agency |
| LAI | Leaf area index |
| LCC | Land cover change |
| LE | Latent heat |
| LOESS | Locally weighted polynomial regression model |
| LP DAAC | Land Processes Distributed Active Archive Center |
| LST | Land surface temperature |
| LW | Longwave |
| MAM | March April May |
| MERRA | Modern-Era Retrospective analysis for Research and Applications |
| METRIC | Mapping evapotranspiration at high resolution with internalized calibration |
| MJO | Madden–Julian Oscillation |
| MODIS | Moderate Resolution Imaging Spectroradiometer |
| MVIRI | Meteosat visible and infrared imager |
| NASA | National Aeronautics and Space Administration |
| NDVI | Normalized difference vegetation index |
| NIR | Near-infrared |
| OECD | Organisation for Economic Co-operation and Development |
| OND | October November December |
| PR | Precipitation Radar |
| PROBA-V | Project for On-Board Autonomy - Vegetation |

| | |
|---|---|
| SEVIRI | Spinning Enhanced Visible and InfraRed Imager |
| SIS | Surface incoming shortwave radiation |
| SPI | Standardized precipitation index |
| SPOT | Satellite Pour l'Observation de la Terre |
| SR | Surface roughness |
| SW | Shortwave |
| SZA | Solar zenith angle |
| TMI | TRMM Microwave Imager |
| TOA | Top-of-atmosphere |
| TRMM | Tropical Rainfall Measuring Mission |
| UNDESA | United Nations Department of Economic and Social Affairs |
| UNOCHA | United Nations Office for the Coordination of Humanitarian Affairs |
| VIRS | Visible and Infrared Scanner |
| VIS | Visible |
| WMO | World Meteorological Organization |

# List of figures and tables

# 1 Introduction

## 1.1 Overview

Climate and vegetation are closely linked. While the distribution and productivity of vegetation are largely determined by climate, vegetation in turn affects the climate through regulating the amounts of water, energy, momentum, and gas exchange with the atmosphere (Hoffman and Jackson et al., 2000; Foley et al., 2005; Davin and de Noblet-Ducoudre, 2010; Pielke et al., 2011). Land surface temperature (LST), which is defined as the radiometric temperature of the land surface, is one of the most important climate variables in the physics of land surface processes, and its magnitude is determined by the interaction between vegetation and the atmosphere (Schmugge and Becker, 1991; Jin et al., 1997; Jin and Dickinson, 2010; Li et al., 2013). LST strongly responds to vegetation–atmosphere interactions during plants' annual growing cycle, as well as perturbations caused by human interventions and climate extremes (Jin and Dickinson, 2010; Richard et al., 2013; Mahmood et al., 2014).

Under normal conditions, the impact of vegetation on the climate system is mainly regulated by seasonal vegetation growing cycles or phenology (Richard et al., 2013). Through structural changes (associated with the development and senescence of the canopy) and physiological changes (e.g., evapotranspiration (ET) and photosynthesis), vegetation phenology affects the seasonality of albedo, surface conductance, and surface roughness (SR) length, which directly influence fluxes in water and energy as well as LST seasonality (Fitzjarrald et al., 2001; Penuelas et al., 2009; Richard et al., 2013). LST is driven by the combined biophysical attributes of the land surface (i.e., albedo, ET, and SR) (Jin et al., 2005). Examining how interactions between vegetation greening and water availability determine LST seasonality is fundamental to understanding how the timings of leaf emergence and senescence affect the climate through their influence on surface energy budget and LST (Penuelas et al., 2009).

Humans perturb vegetation–atmosphere interactions by altering the biophysical attributes of the Earth's surface through land cover change (LCC). Since 1700 AD, approximately 12 million $km^2$ of natural vegetation (forest and woodland) have been cleared globally (Ramankutty and Foley, 1999); furthermore, as of 2014, the area affected directly by human activities had reached approximately 100 million $km^2$, 18–29% of which was cleared mainly though deforestation for agricultural, urban, and infrastructural use (Luyssaert et al., 2014). Agricultural expansion, however, was the major driver of global land use and LCC, because urban landscapes constitute a smaller area of the total land surface (< 5%) (Pielke et al., 2011). Such massive transformations of land cover have had considerable impacts on the climate locally (Arnfield, 2003; Lee et al., 2008), regionally (Mohr et al., 2003; Foley et al., 2003a), and globally (Davin and Noblet-Ducoudre, 2010; Lawrence et al., 2010; Duveiller et al., 2018).

Although the global pace of LCC has slowed in recent decades, tropical regions still have the highest rate of loss (e.g., an annual forest loss rate of 2101 $km^2$) caused by rapid agricultural expansion (Hansen et al., 2013; FAO, 2012). The net impact of this global LCC showed an average increase in LST, and the warming behind this transition was attributed to agricultural expansion in the tropics (Duveiller et al., 2018).

In Sub-Saharan Africa, the agriculture sector plays a critical role in the economy, employing more than half of the total work force (OECD/FAO, 2016); between 1975 and 2000, crop land increased by 57% at the cost of natural vegetation (forest, woodlands, and bushland) (Brink and Eva, 2009). This trend is more prevalent in East Africa, where between 2002 and 2008 alone forest and woodland cover declined by 5% and 15.8% respectively (Pfeifer et al., 2012).

For a full understanding and successful mitigation of the climatic impacts of LCC, biogeophysical impacts should be accounted for along with biogeochemical effects (Pielke, 2011; Bright et al, 2015; Devaraju et al., 2015). Although these biogeochemical effects (e.g., CO2 emissions) are largely studied and well recognized in existing impact assessment reports of the Intergovernmental Panel on Climate Change (IPCC), the biogeophysical impacts (e.g., non-radiative components) have not been fully addressed (e.g., regionally and seasonally) in these reports (Myhre et al., 2013; IPCC, 2019). Biogeophysical impacts are stronger at regional and local scales and can have remote effects through their influence on atmospheric circulation patterns (Henderson-Sellers et al., 1993; Devaraju, 2015). Moreover, their influence can vary across space, and in some regions they can have a similar or larger magnitude than greenhouse gas-induced climate change (Bonan, 2008b; Feddema et al., 2005; Avila et al., 2012); in addition, they can amplify or counteract greenhouse gas effects (Mahmood et al., 2014). Failing to include biogeophysical impacts in life cycle assessments can lead to unproductive climate change mitigation and adaptation measures in regions of intensive LCC (Pielke et al., 2011; Bright, 2015). Hence, further studies are required locally and regionally to support initiatives and policies for the successful mitigation of climate change effects.

Climate extremes are another factor that disturbs climate–vegetation interaction. In a water-limited environment, the surface feedback caused by soil moisture and vegetation stress during drought events alters the surface energy balance through modifying surface biophysical properties; this in turn increases surface and air temperatures, amplifying the effect of drought (Fischer et al., 2012; Yin et al., 2014). According to the Fifth Assessment Report of the IPCC, climate extremes such as droughts and floods remain formidable challenges in the 21st century. Furthermore, temperatures are projected to rise faster than the global average increase (0.85°C) in Africa. Globally, up to 40% of the world's population live in regions that have already experienced warming of > 1.5°C (Allen et al., 2018; IPCC special reports on global warming). Hence, under the impact of global warming and climate extremes, understanding how different ecosystems respond to precipitation extremes and the role of vegetation in modulating or amplifying surface warming must be explored further for informed decision-making in climate change mitigation efforts.

Eastern Africa (EA) is one of the regions most affected by factors that disrupt climate–vegetation interaction. Because of the rapid agricultural expansion associated with fast population growth, land cover in East Africa has undergone a considerable transformation. By 2050, if the current trend persists, the population is expected to double in this region (UN DESA, 2019), posing further pressure on the already degraded natural landscape. Concurrently, with an increase in drought and flood frequency in the region, climate patterns are becoming more erratic and rainfall highly variable (Nicholson, 2017); this will severely limit vegetation productivity and affect the surface energy balance and LST in the region. Therefore, understanding

how different ecosystems respond and affect the climate system during LCC and climate extremes is critical in this region to devise effective mitigation measures and strategies.

The scarcity of in situ data is a major barrier to better understanding the climatic impacts of vegetation dynamics in Eastern Africa. The occurrence of FLUXNET, a global network of micrometeorological flux towers that measures exchanges of water and energy between the terrestrial ecosystem and atmosphere, is rare in this region. Consequently, methods and models that make use of high-quality satellite observation data are required. This thesis presented a combination of interdisciplinary studies, including remote sensing, climatology, atmospheric science, forestry, ecology, geography, and geographic information science. The thesis applied statistics and various empirical and energy balance-based models driven by satellite observations and meteorological data, with the aim of answering how vegetation dynamics affect the surface energy balance and LST in the EA.

## 1.2 Objectives

The main objective of this thesis is to clarify the biophysical mechanisms through which vegetation dynamics affect LST in the Eastern Africa. This thesis is aimed at improving the understanding of climate–vegetation interactions to support climate change mitigation and land management efforts. The main objective is divided into the following four specific objectives:

i. To identify the role of seasonal vegetation-rainfall dynamics on LST patterns;

ii. To quantify the impacts of multiple LCCs on LST;

iii. To clarify the relative contributions of the radiative and non-radiative mechanisms to LST changes during LCCs;

iv. To evaluate the energy exchange and LST sensitivity during precipitation extremes across biomes.

These objectives are addressed in four interrelated research papers (Figure 1). The contents of each paper (I–IV) are summarized as follows.

**Paper I** aimed to identify the impacts of rainfall–vegetation interaction on LST seasonality as well as how such interactions affect LST anomalies under forest loss and drought events in the Horn of Africa (HoA). This study further examined how vegetation vigor (greenness) affects temperature anomalies during major drought events. Time series data (2001–2016) from satellite observation were used and all analyses were conducted at 1-km resolution. A locally weighted polynomial regression model (LOESS) was fitted to the time series data to model the seasonality of rainfall and vegetation patterns after its applicability was tested in known areas of unimodal and bimodal rainfall. The LST seasonality was then assessed for the corresponding location within rainfall–vegetation space during seasonal growing cycles, as well as under perturbations from forest loss and drought events. Verified forest loss sites in Ethiopia and Kenya were used for the case study.

**Paper II**'s objective was to elucidate the impacts of growing-season albedo and ET dynamics on radiation balance and LST as well as quantify the biophysical effects of multiple LCCs across seasons and biomes in the Horn of Africa (HoA). The effects of actual LCCs on regional radiative forcing and LST were

analyzed across seasons for all vegetated surfaces during 2001–2013. The relative contributions of radiative (albedo) and non-radiative (ET and SR) mechanisms to the change in LST were quantified using the Intrinsic Biophysical Mechanism (IBPM) method (Lee et al., 2011) together with various empirical models. The impacts of interannual climate variability and background climate signals on the LST were removed from all pixels. All analyses were performed using satellite observation and meteorological reanalysis data from 2001–2013 at 1-km resolution.

**Paper III** examined energy exchange and LST anomalies during 2001–2016 precipitation extremes in the HoA across multiple ecosystems and seasons. Specifically, how spectral albedo in the broadband visible (VIS), near-infrared (NIR), and shortwave (SW) range responded to rainfall extremes and their consequent influence on surface–atmosphere coupling through radiative forcing were analyzed. Moreover, turbulent and radiative energy exchange and LST anomalies were compared across biomes. To assess changes caused by precipitation extremes alone, the impacts of other factors that concurrently affected energy exchange and LST (e.g., LCC) were discarded from the analysis. Furthermore, the 3-month standardized precipitation index (SPI), surface energy balance, and quantile regression analysis were applied to satellite observation data at 0.05° (approx. 5 km) resolution.

**Paper IV** was based on the limitations identified in Paper II and explored small-scale biophysical impacts in depth with the objective of investigating the impacts of bushland-to-cropland conversion on surface energy balance and LST in southern Kenya. Although bushland (Acacia-Commiphora) constitutes the largest ecosystem in EA, the biophysical impacts of its conversion to cropland were uncertain because changes occur in fragmented and small patches, making identifying them difficult at coarse resolutions. This paper presents a new perspective on their potential impacts on LST using inputs from high-resolution satellite images, ground meteorological station data, and land surface flux modeling approaches at two selected sites (Mwatate and Ndome) in southern Kenya. Blue-sky (actual albedo) was derived from Landsat 8 and MODIS Bidirectional Reflectance Distribution Function (BRDF) anisotropy data; energy fluxes were estimated using the mapping evapotranspiration at high resolution with internalized calibration (METRIC) model; and energy balance decomposition was performed to measure changes in each of the energy balance terms and their contribution to the average LST difference.

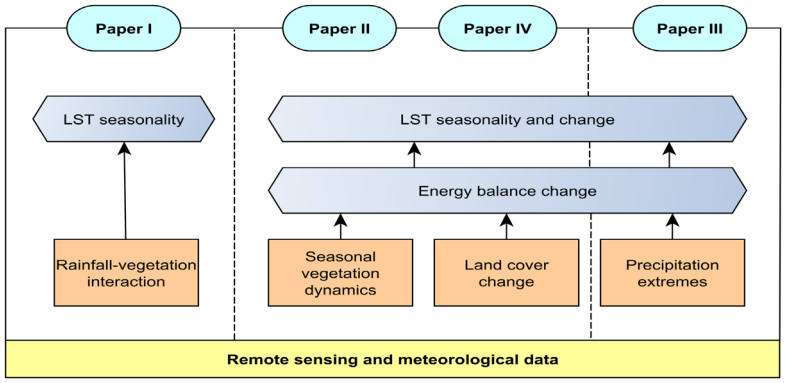


**Figure 1.** Relationships between papers (I–IV) based on their key areas of research and data source.

# 2 Background

## 2.1 Geographical context

This thesis covers five countries (Ethiopia, Eritrea, Djibouti, Somalia, and Kenya) located in the Eastern-most parts of Africa, commonly known as Horn of Africa (HoA). The studies conducted for Papers I–III were regional and covered the whole HoA (Figure 1a). For Paper IV, local scale studies were conducted in the Taita Hills of southern Kenya (Figure 1b).

The study area exhibits high diversity in topography, climate, and vegetation. The topographic elevation ranges from 125 m below sea level at the Danakil Depression in Ethiopia to 5199 m above sea level at Mount Kenya. Temperature reaches as low as 12°C at mountain summits and rise to 34°C in the lowlands. The lowlands, which cover a large part of the region, are characterized by a dominantly semiarid climate; rainfall here can be as low as 200 mm, whereas in the highlands it often exceeds 1500 mm and exhibits high spatial differences within short distances under a strong orographic influence (Nicholson, 1996).

In addition, the annual rainfall cycle exhibits variations across the region. Owing to the biannual equatorial passage of the Intertropical Convergence Zone (ITCZ), much of the region receives a bimodal rainfall during March–May ("long rains") and October–December ("short rains"). However, small portions in central-western Ethiopia receive a unimodal June–August rainfall (Lyon 2014). Since 1999, a considerable decline in the March–May rainfall trend has been noted (Funk et al., 2005; Lyon and DeWitt, 2012). Although the causes of this decline are controversial, studies have implicated the warming of the Indian and Pacific Ocean (Funk, 2014; Rowell et al., 2015). Moreover, rainfall patterns in the region are characterized by strong interannual and intraseasonal variability associated with El Niño–Southern Oscillation (ENSO), the Indian Ocean Dipole (IOD), and the Madden–Julian Oscillation (MJO) (Nicholson, 2017). In recent years, recurrent and prolonged droughts have prevailed in the region and at times caused a total failure of the October–December rains, such as in 2010 (Uhe et al., 2018).

Various ecoregions (Somali-Masai, Sudanian, Zanzibar Inhambane, and Afromontane) cover the HoA, and are associated with climatic and topographic heterogeneity in the region. The Somali-Masai ecoregion, dominated by bushland and thickets, covers the largest area and occupies eastern Eritrea, southern Ethiopia, and large parts of Somalia and Kenya (White, 1983; Bouvet et al., 2018). The tree species Acacia and Commiphora constitute the bushland and thickets, which are deciduous in the lowlands and grade into semi evergreen and evergreen on the foothills of the mountains in the region. Although smaller in area, shrubland, grassland, and riparian forest also make up this ecoregion (White, 1983). The Sudanian ecoregion, which extends from neighboring Sudan, covers up to the foothills of the Ethiopian Highlands in the west. Mainly woodland and grassland constitute this ecoregion. The Zanzibar Inhambane and Afromontane ecoregions represent a small area in the region; the former occurs along the southern and eastern periphery of Somalia and Kenya and is characterized by mosaics of shrubland, thickets, scrub forest, and wooded grassland, whereas the latter occurs in the highland mountains of Ethiopia and Kenya, and is characterized by forest..

Over the last few decades, these ecoregions

have faced considerable anthropogenic pressure from rapid agricultural expansion in the region. For instance, between 1990 and 2010, the cultivated area increased by 28% at an annual rate of 1.4%, mainly at the expense of wooded natural vegetation such as forest, woodland, bushland, thicket, and shrubland (Pfeifer et al., 2012; Pellikka et al., 2013; Brink et al., 2014). With an increasing population and consequent demand for greater crop production, more woodland is expected to be converted to cropland in the region (Maeda, 2011).

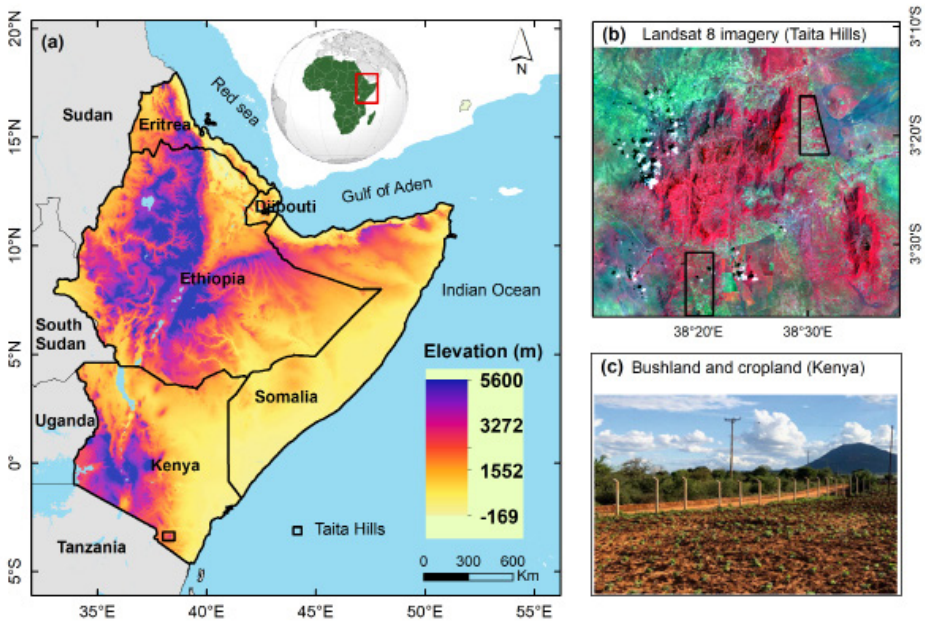


**Figure 2.** (a) Location of the study area with the GTOPO30; (b) Landsat 8 false color composite (acquired November 27, 2014) showing Taita Hills and locations of study areas in the lowlands; (c) Bushland (Acacia-Commiphora) and adjacent commercial cropland in Taita lowlands with Mbololo mountain in the background. Photo: Petri Pellikka, 2019.

## 2.2 Rainfall-vegetation interaction and its impact on climate

Vegetation seasonality largely depends on rainfall in arid and semiarid areas, where water is a limiting climatic factor (Zhang et al., 2005). This is particularly critical in regions where food production and security rely heavily on rainfed agriculture. Under the growing impact of climate change on rainfall, large bodies of studies have explored the relationship between rainfall and vegetation seasonality using remote sensing observations (e.g., Zhang et al., 2005; Camberlin et al., 2007; Hawinkel et al., 2016). Remote sensing is defined in this thesis as the science and art of obtaining information about an object, area, or phenomenon through analyzing data acquired from a distance using sensors mounted on satellites or aircraft (Lillesand and Kiefer, 1979). Remote sensing satellite observations are often used in rainfall and vegetation seasonality studies because of their advantages of wider spatial coverage (local to global), high spatial resolution (showing details ranging from a few km to a submeter scale), and high temporal resolution (capturing changes up to daily time steps through a shorter revisit cycle). However, despite these studies, the role of rainfall–vegetation interactions in determining LST seasonality remains uncertain because concurrent human impacts on vegetation and climate extremes complicate such interaction. Understanding how vegetation impacts LST seasonality requires the underlying biophysical mechanisms driving the changes to be clarified. LST seasonality is directly affected by radiative (albedo), physiological (e.g., ET), and aerodynamic (e.g., SR) changes during seasonal vegetation growing cycles or phenology in deciduous ecosystems (Richard et al., 2013; Figure 3).

Surface albedo is one of the key parameters through which vegetation directly affects the climate system (Richard, 2013). Albedo, defined as the fraction of incident solar radiation reflected by the land surface, affects the local and global climate through its influence on radiation balance at the surface and top-of-atmosphere (TOA) levels (Otterman, 1977, Dickinson, 1983; Davin and De Noblet-Ducoudre, 2010). Albedo varies among vegetation types; for example, forests mostly have lower albedo than do croplands or other shorter vegetation, and tend to appear darker and absorb more radiation. During canopy development and senescence, marked differences in albedo occur seasonally during leaf-out, peak greening, and leaf-off due to differences in the reflectance of visible (VIS) and near-infrared (NIR) radiation, which are associated with leaf area index (LAI), canopy height, and fractional canopy cover changes (Moore et al., 1996; Ryu et al., 2008; Hollinger et al., 2010). Moreover, the seasonal pattern of albedo is influenced by the solar zenith angle (SZA) and background material (e.g., soil color and moisture content) in deciduous ecosystems (Campbell and Norman, 1998; Song et al., 1999).

Additionally, through ET and SR, vegetation further affects energy and water fluxes from the land surface to the atmosphere. ET is a process through which water is transferred from the surface to the atmosphere through evaporation (e.g., from soil, canopy interception, and water bodies) as well as transpiration from plants. This process directly affects the climate through modulating the latent heat (LE) flux to the atmosphere. By contrast, SR indicates the roughness of the land surface as determined by the canopy height (Shaw and Pereira,1982) and LAI (Lindroth, 1993; Raupach, 1994). SR is an important surface parameter that affects the

turbulent mix of air and the transport of heat and moisture from the surface to the atmosphere (Bonan, 2015). When moving air meets a rough surface (e.g., forest), the speed at which momentum is transferred from the atmosphere to the surface reduces. This, in turn, creates a turbulent mix of air and the transport of sensible (H) and LE from the surface to the atmosphere, leading to a decrease in temperature (Hoffmann and Jackson, 2000; Bonan, 2015).

## 2.3 Biophysical impacts of land cover change

The biophysical impacts of LCC vary with the type of LCC, geographic location, scale of study (i.e., local, regional, or global), and season (see Perugini et al., 2017 for an extensive literature review). According to the Fifth Assessment Report of the IPCC, historical anthropogenic land cover has increased the albedo of the Earth with a radiative forcing of $-0.2 \pm 0.2$ W m$^{-2}$ relative to preindustrial levels (Myhre et al., 2013). Despite the global cooling effect from increased albedo, the report concludes that no consensus exists on the sign of the net temperature change from anthropogenic LCC because the non-radiative impacts (ET and SR) are uncertain (Myhre et al., 2013).

Modeling and observational studies have shown two opposite biophysical effects following deforestation: a surface-cooling effect caused by an albedo increase and a surface-warming effect caused by concurrent decreases in ET and SR. The net effect (warming/cooling) is determined by the relative strength of these contrasting changes and varies with latitudes. In the boreal zone, the albedo impact dominates and results in net cooling, whereas in the tropics the non-radiative effect dominates, leading to net warming on average (Alkama and Cescatti, 2016). By contrast, in the temperate zone, changes in magnitude are comparable and the sign of net temperature change is uncertain because observation and modeling have shown contrasting results (Pitman, 2006; Lee et al., 2011; Li et al., 2015a; Alkama and Cescatti, 2016; Li et al., 2016; Perugini et al., 2017). However, it is evident that local or regional biophysical climate impacts are stronger in magnitude than global effects because the biophysical mechanisms are highly influenced by location-specific environmental factors (Bright et al., 2017; Perugini et al., 2017). Therefore, further studies at the local and regional level are highly relevant for guiding land use policies and implementing effective climate change mitigation and adaptation strategies.

The impacts of LCC are currently assessed using either modeling or observational studies. The capacity of global models to accurately reproduce local climate effects and represent the climatic impacts of LCC is still highly limited because of their coarse spatial resolution and uncertainties in physical processes, parameterization, and input data (Li et al., 2015a; Duveiller, 2018). Because of this, contradicting predictions have been observed in model-based studies (Pitman et al., 2009; Boiser, 2012), and hence, more observational studies are required. Currently, observational studies are based on in situ or satellite data. Although in situ measurements from field experiments or global networks of flux towers (e.g., FLUXNET) provide local evidence to verify modeling results, they represent only small geographic locations and land cover types, and hence are insufficient to address the spatially heterogeneous biophysical properties and climatic conditions worldwide (Duveiller, 2018). Consequently, following recent advances in remote sensing technology, satellite observation-based studies are increasing

as such data provide repetitive observations of a wider geographic area with high spatial and temporal resolution.

Observation-based biogeophysical metrics that are used to quantify the impact of LCC on climate can be divided into two categories: the first focuses on the albedo impact of LCC, whereas the second focuses on temperature impacts of LCC. The albedo effect is quantified using shortwave radiative forcing (Betts, 2000; Pielke et al., 2002; Bright et al., 2015). Bright et al. (2015) proposed a simple method for quantifying the radiative forcing at the surface and TOA levels. At the surface level, radiative forcing is given by the product of albedo change and local incoming solar radiation incident at the surface, whereas at the TOA level, it can be approximated using information on the upwelling atmospheric transmittance of shortwave radiation and the fraction of the Earth's surface area affected by albedo change.

Metrics that emphasize temperature impacts of LCC can further be divided into two subgroups. The first subgroup measures temperature changes without separately quantifying the contributions of each biophysical factor (i.e., albedo, ET, SR) to the observed temperature change (e.g., Li et al., 2015a; Alkama and Cescatti et al., 2016). This approach measures the temperature change attributed only to LCC by removing the effects of interannual climate variability and local background climate signals from the analysis using adjacent stable pixels unaffected by LCC. The second subgroup focuses on attributing and quantifying the temperature change to various biophysical effects, which are based on surface energy balance equations (Lee et al., 2011; Luyssaert et al., 2014). The IBPM method developed by Lee (2011) breaks down the biophysical effects into radiative forcing terms and nonradiative terms, which are comprised of additive components from Bowen's ratio and SR. The other method proposed by Juang et al. (2007) and elaborated by Luyssaert et al. (2014) provides energy balance decomposition (EBD) to attribute the temperature change caused by each of the energy balance terms. Compared with the first category, such decompositions of temperature contributions in IBPM and EBD capture temperature changes and biophysical feedbacks well and have crucial benefits for understanding the underlying physical mechanisms, assessing the performance of climate models, and developing strategies to mitigate climate warming (Chen & Dirmeyer, 2016; Rigden and Li, 2017).

In EA, the local and regional biophysical impacts of land cover type are uncertain since global studies are too coarse to capture local effects. For example, despite bushland (Acacia-Commiphora) being the largest ecosystem in the region and currently facing considerable pressure from cropland expansion, its biophysical impacts on the climate are poorly understood. Thus, a comprehensive evaluation of biophysical impacts is urgently required for effective land use planning and climate change mitigation strategies.

## 2.4 Energy exchange and surface feedbacks during precipitation extremes

With a projected increase in extreme events and global temperatures, the impacts and risks associated with climate change are expected to intensify (IPCC, 2013). Studies have suggested that extreme events were largely initiated by external large-scale circulation anomalies (i.e., sea surface temperature anomalies); however, land surface feedback also played important role through intensifying extreme events (Folland et

al., 1986; Notaro et al., 2019).

During precipitation extremes, the degree of surface feedback on the climate varies among vegetation types and regions (Pielke, 2001; Anderegg et al., 2019). Vegetation affects the climate through regulating the dissipation of energy and water fluxes to the atmosphere (Figure 3). The regulating capacity differs among vegetation types because of variations in plants' physiology, structures, and survival mechanisms. For example, grasses, which have relatively shallow rooting systems, quickly dry out, whereas forests can access water from deep soil layers, reduce soil moisture deficits through hydraulic lift, and withstand prolonged drought periods through stomatal closure and osmotic adjustment (Baldocchi et al., 2004). These differences have direct impacts on the partitioning of turbulent fluxes and the intensification of drought. For instance, as ET declines following soil desiccation and vegetation dry-out, much of the incoming radiation will be used to warm the environment, because available energy is converted to H (instead of LE). Progressive ET reduction and accumulation of H flux in the atmosphere lead to the drying and warming of the atmospheric boundary layer, further intensifying drought events through impeding cloud formation (Miralles et al., 2019).

In addition, surface albedo changes affect the energy budget following vegetation and soil moisture stress during droughts. Modeling studies have reported positive vegetation–rainfall feedback through albedo changes (Charney, 1975; Meng et al., 2014), whereas observational studies have challenged whether albedo changes are strong enough to affect surface–atmospheric coupling (e.g., Teuling et al., 2008). During a European drought, Teuling et al. (2008) revealed contrasting changes in VIS and NIR albedo in forest and wooded savanna, which largely limited SW albedo changes. However, drought-period spectral albedo patterns (VIS, NIR, and SW) and their impacts on the energy budget are unknown in arid and semiarid environments that are dominated by shrublands and grasslands, such as in the EA.

In recent decades, EA has been affected by frequent drought and flood events. Associated with fast population growth and the agriculture sector's strong dependence on seasonal rainfall, the socioeconomic vulnerability of the region to hydroclimatic extremes is high, as evidenced by their considerable impacts on humans (i.e., food shortages, famine, and loss of life) and property (UNOCHA, 2011; Lyon and DeWitt, 2012). To mitigate the impacts of drought, studies have proposed various geoengineering solutions, including afforestation, reafforestation, forest protection, irrigation, and targeted modification of surface albedo (Bonan, 2008; Hirsch et al., 2017; Seneviratne et al., 2018). However, for implementing effective mitigation measures, hot-spot areas should be identified, and the various mechanisms that can amplify drought and intensify surface warming need to be comprehensively assessed. For this purpose, given the physiological and structural differences between the different types of vegetation, understanding and evaluating ecosystem-specific responses of energy exchanges, which are lacking in EA, are critical for devising effective mitigation plans (Teuling et al., 2010; Miralles et al., 2019).

# 3 Data

## 3.1 Satellite observation data

In this thesis, a large set of satellite observation data were used, primarily from the MODIS. Table 1 presents a summary of these data. All MODIS data were downloaded from the Land Processes Distributed Active Archive Center (LP DAAC) NASA. In Papers I–III, the MODIS LST product MOD11A2 was used. MOD11A2 LST data were prepared from the 8-day average of a daily LST product (MOD11A1), which was retrieved using a generalized split-window algorithm under clear-sky conditions (Wan, 2014). A quality assurance (QA) layer was used in this product to filter clear-sky retrievals using QA bit flags. Through this process, only pixels with average LST errors ≤ 1K were selected for analysis (Wan, 2015). For detailed information about LST, please refer to Paper I.

The BRDF/Albedo model, which provides the weighting parameters (isotropic, volumetric, and geometric) required for calculating the albedo and reflectance at desired sun and sensor view angles, was used in all papers. In Papers I–III, it was used to remove sun-sensor view angle effects (BRDF effects) on the directional reflectance in enhanced vegetation index (EVI) calculations through fixing the sensor angle at a nadir and the sun angle at 45°. In Papers II and IV, it was also used in the computation of blue-sky (actual) albedo together with aerosol optical depth data. Furthermore, black-sky albedo at local noon was used in Papers II and III. Validations of albedo products with ground measurements were reported to have an accuracy than 5% for areas with an SZA below 70° (Liu et al., 2009).

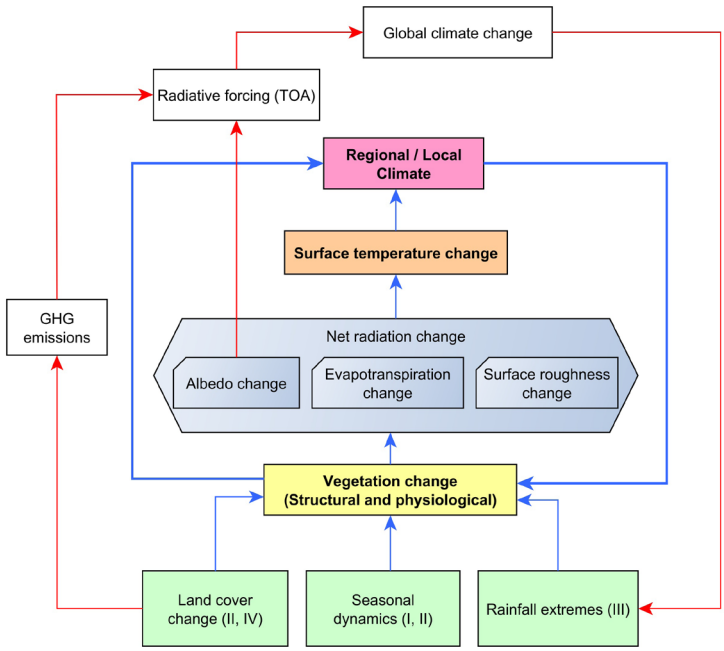


**Figure 3.** Conceptual flow chart presenting the impacts of vegetation changes—induced by anthropogenic and natural causes—on the climate system through biophysical changes; shaded boxes and blue lines are topics and interactions, respectively, addressed in Papers I–IV. TOA is top-of-atmosphere; GHG is greenhouse gas.

**Table 1**. Summary of satellite observation data used in Papers I–IV.

| Data type | Sensor | Product | Paper |
|---|---|---|---|
| BRDF/Albedo model | MODIS | MCD43B1; MCD43C3; MCD43A1 | I, II, IV |
| Black sky albedo | MODIS | MCD43B3; GLASS Albedo | II |
| Land surface tempera-ture/emis-sivity | MODIS | MOD11A2; MOD11B3 | II, III |
| Leaf area index | MODIS; SPOT-vegetation and PROBA-v | MCD15A2H; LAI | II, III |
| Evapotranspiration | MODIS; Mod-elled from different satellites | MOD16A2; GLEAM | II, III |
| Vegetation cover | MODIS | MCD12Q1; MOD44B | II |
| | | GLC-SHARE | I |
| Forest change | Landsat | Global For-est Change | I, II |
| Aerosol optical depth | MODIS | MCD19A2 | IV |
| Rainfall | TRMM | 3B43 | I, II, III |
| Elevation model | ALOS | AW3D30 | IV |
| Radiation | MVIRI/SEVIRI; CERES | Heliosat (SARAH); EBAF | II, III |
| Multispectral imagery | Landsat 8 OLI/TIR; RapidEye | C1 Level-1 and C1 level-2 | IV |

Leaf area index products from the MODIS (Paper II) and SPOT-vegetation and PROBA-V sensors (Paper III) were used for inferring vegetation dynamics during growing periods and precipitation extremes, respectively. The MODIS LAI was preprocessed to filter best-quality retrievals of pixels without saturation using quality flags (Yang et al., 2006); the latter was reported to have better accuracy compared with MODIS LAI—particularly in high biomass areas (Li et al., 2015b)—and 90% of its samples met the Global Climate Observing System accuracy requirements (Verger et al., 2014). It can be downloaded for free from Copernicus Global Land Service.

Evapotranspiration products from the MODIS and Global Land Evaporation Amsterdam Model (GLEAM) were used in Papers II and III, respectively. The gap-filled MODIS ET was prepared from daily meteorological data in combination with other MODIS products (albedo, LAI, and land cover) using the Penman–Monteith equation (Running et al., 2017). Validation of this product against flux tower data revealed an accuracy of approximately 0.3 mm day-1 (Running et al., 2017). Furthermore, GLEAM ET data, which use the Priestley and Taylor evaporation model (Martens et al., 2017), were downloaded from https://www.gleam.eu/. This product correlated well (R = 0.81) with eddy-covariance measurements (Martens et al., 2017). For analysis, GLEAM ET was preprocessed to retrieve LE flux using Dingman (2015) equations (Paper III).

In addition, radiation flux data from Meteosat Visible and InfraRed Imager (MVIRI)/Spinning Enhanced Visible and InfraRed Imager (SEVIRI) (Paper II) and Clouds and the Earth's Radiant Energy System (CERES) (Paper III) were used. In Paper II, only surface incoming shortwave radiation (SIS) from the visible channels of

MVIRI/SEVIRI onboard the Meteosat satellite was downloaded from the European Organisation for the Exploitation of Meteorological Satellites (EUMETSAT) Climate Monitoring Satellite Application Facility (CM SAF). A comparison of SIS against in situ measurements showed an average absolute bias of 5 W $m^{-2}$ (Pfeifroth et al., 2017). In Paper III, both the incoming and upwelling shortwave (SW) and longwave (LW) radiation fluxes from the CERES Energy Balanced and Filled (EBAF) product, downloaded from NASA, were used. CERES-derived irradiances are stable over long periods with an uncertainty of approximately 0.5 W $m^{-2}$ per decade (Loeb et al., 2012).

Land cover data from the MODIS, with International Geosphere-Biosphere Programme (IGBP) land cover classification schemes, were used in Papers II and III. This product was derived from a supervised classification of MODIS (Terra and Aqua) reflectance and has an accuracy of around 75% (Friedl et al., 2010). In addition, percentage of vegetation fractions were inferred from the Vegetation Continuous Fields product (MOD44B) in Paper III. Other sources of land cover data (e.g., a global land cover database from the Food and Agriculture Organization (FAO) of the United Nations and a Landsat-based forest cover change product from the University of Maryland (Hansen et al., 2013) were also used in Paper I.

In Paper IV, high-resolution data from Landsat 8 (30 m), RapidEye imagery (5 m), and an elevation model (30 m) were used to estimate small-scale biophysical changes associated with LCC. Prior to being used for analysis, clouds, cloud shallows, and cirrus were masked from Landsat 8 scenes using the QA band. In addition, topographic effects were removed from the surface reflectance by applying C-correction (Teillet et al., 1982) using gap-filled digital elevation from the Japan Aerospace Exploration Agency (JAXA). The RapidEye imagery obtained from https://www.planet.com/ is a level 3A orthorectified product; it was atmospherically corrected using the Fast Line-of-sight Atmospheric Analysis of Hypercubes (FLAASH) algorithm in the Environment for Visualizing Images (ENVI) software before being utilized for the analysis.

In Papers I and III, rainfall data from the Tropical Rainfall Measuring Mission (TRMM) were used to quantify the intensity of precipitation extremes. This product was downloaded from NASA (https://pmm.nasa.gov/data-access/downloads/trmm). It combines multiple independent precipitation estimates from high-quality microwave (TRMM Microwave imager (TMI), infrared (Visible and Infrared Scanner (VIRS)), radar (precipitation radar (PR)), lightning (Lightning Imaging Sensor), CERES, and rain gage data. The TRMM has been extensively validated at various sites worldwide (Fleming et al., 2011; Cao et al., 2018) and has been reported to have good agreement with gage data, including in Africa (Adeyewa and Nakamura, 2003; Nicholson et al., 2003). Moreover, the TRMM showed better performance compared to other gridded precipitation data for drought monitoring in Africa (Naumann et al., 2012).

In each paper, all data were spatially and temporally harmonized prior to use for analysis. The spatial harmonization was at 1-km (Papers I and II), 5-km (Paper III), and 300-m (Paper IV) resolutions.

## 3.2 Meteorological data

The meteorological data utilized were the reanalysis air temperature (Papers II and III) and weather station data (Paper IV). For the air temperature reanalysis data, the Modern-

Era Retrospective analysis for Research and Applications (MERRA-2) product was used. This product was downloaded for the 2001–2013 period from the Global Modeling and Assimilation Office of NASA. The screen level (2 m) air temperature product was prepared from combined weather and satellite data and reported to have a daily average bias of 0.1 K compared with in situ data over land surfaces (Michael et al., 2015).

Furthermore, weather station data for two sites in southern Kenya (Maktau and Voi) were obtained from the University of Helsinki and Kenya Meteorological Department. The Maktau automatic weather station data were applied for ET estimation in the METRIC model, and the Voi data were applied for comparing the modeling results. The data records for both sites were complete for the analyzed periods (2014–2018).

# 4 Methods

## 4.1 Identifying impacts of rainfall-vegetation interaction on land surface temperature

Two steps were followed to identify how rainfall–vegetation interaction affects LST in the region (Paper I). The first step was to explore this interaction through modeling the relationship between rainfall and vegetation seasonality. For this, local maxima of rainfall and EVI distribution were identified by fitting a nonparametric locally weighted polynomial regression model (LOESS) on their seasonality curve (2001–2016). The model was integrated with a peak identification function, which identifies local maxima using rainfall or EVI climatology for each pixel by selecting a peak whose value is at least twice as high as neighboring values in the time seasonality curve. This criterion was defined after its applicability was tested in areas with known unimodal (one peak) and bimodal (two peaks) rainfall patterns in the region. Once the local maxima were obtained, rainfall and EVI modality patterns were compared for every pixel to understand to what extent vegetation follows rainfall seasonality patterns across the region. Furthermore, relationships between EVI and rainfall climatology were explored statistically using the nonparametric Spearman coefficient.

The second step was to evaluate how rainfall–vegetation interaction affects LST seasonality. Representative samples from each of the major natural vegetation types (shrubland, grassland, and forest) were selected. The samples (10 × 10 km), one from a unimodal area and the other from a bimodal one, were chosen from each vegetation class where rainfall–EVI correlation was strong ($r \geq 0.8$). For those sample areas, the climatology of EVI and LST were studied for both the unimodal and bimodal areas; moreover, to show how LST interacts with EVI and rainfall, EVI (y-axis) and rainfall (x-axis) relationships were classified using the corresponding LST value. Furthermore, to understand how different intensities of EVI and rainfall interaction affect LST, two strong drought events were selected (2010/2011 and 2015) and interactions were tested in the region. For this, standardized anomalies of rainfall and EVI were classified according to the LST anomaly in a scatterplot. Then, the mean LST anomaly for the corresponding EVI and rainfall anomaly bins were calculated to show their relative effect.

## 4.2 Investigating effects of vegetation seasonality on energy budget, and land surface temperature

To identify the impacts of vegetation seasonality on albedo and energy budget, first a representative stable sample area (3 × 3 km) was

selected from four dominant natural vegetation types (shrubland, grassland, savanna, and forest) (Figure 1 in Paper II). The stability of the sample areas during the entire time series (2001–2013) was checked using the methodology described in Section 4.3. The climatologies of 8-day composite LAI and shortwave black-sky albedo were computed from 2001–2013 MODIS data for the sample areas and plotted for the four vegetation classes (see Figure 2 in Paper II). The robustness of the results was checked using multiple samples, an alternative dataset for albedo from the Global Land Surface Satellite (GLASS), and through comparing the effects of SZA variation on black-sky albedo. Finally, the maximum impacts of vegetation seasonality on albedo were approximated from albedo differences between growing-season maxima and nongrowing-season minima. Their consequent effect on net shortwave radiation ($\Delta S\alpha$) was computed from the monthly climatology of incoming shortwave radiation (SWin) and the maximum albedo change between the growing and nongrowing seasons ($\Delta\alpha$) using Eq. 1.

$$\Delta S_{(\alpha)} = SW_{in} \times \Delta\alpha \quad (1)$$

The monthly impact of albedo changes on the energy budget was also assessed via its influence on monthly net shortwave radiation (SWnet(i)):

$$SWnet(i) = (1 - \alpha(i)) \times SW_{in(i)} \quad (2)$$

where $\alpha(i)$ is the monthly albedo, and SWin(i) is the monthly incoming shortwave radiation in W $m^{-2}$. The residual available energy for heating the land surface (RE(i)) was computed from SWnet(i) minus ET(i) (the monthly evapotranspiration in W $m^{-2}$ ).

Relationships between vegetation seasonality (inferred from LAI) and albedo, albedo and LST, and LST and ET across space and time were further explored using nonparametric seasonality correlation for every pixel in the HoA. A multiple regression model was tested to identify the impacts of albedo and ET on LST. In areas where albedo and ET exhibited opposite relationships, the net impact on shortwave (SW) radiation and residual energy and their subsequent effect on LST seasonality were assessed using monthly climatology changes.

## 4.3 Quantifying biophysical impacts of land cover change

Two approaches were followed for identifying the actual and potential biophysical impacts of LCC. The actual impacts were measured based on actual LCCs identified from changes in stable land cover maps during the first 5 (2001–2005) and second 5 years (2009–2013) using the MODIS 2001–2013 product (Paper II). The purpose of focusing on stable pixels over 5-year periods was to reduce the impacts of inherent data source (MODIS land cover) classification accuracy on the analysis. For identifying stable pixels during the initial and final 5 years, all land cover layers (2001–2013) were first spatially stacked and the frequencies of all land cover classes were calculated for each pixel. Pixels that were stable for at least 3 years during the initial and final 5 years (i.e., frequency >= 3) were considered stable, otherwise they were discarded from the analysis. Subsequently, LCCs were determined by comparing the two stable maps. In Paper III, a similar procedure was applied to select highly stable pixels during 2001–2016.
In Paper IV, the second approach (space-for-time) was used to estimate potential biophysical impacts by comparing adjacent cropland and bushland within a 300 × 300 m grid. The adjacent bushland and cropland were identified by applying a supervised image segmentation on high-resolution satellite imagery (RapidEye) followed by a pixel-by-pixel verification using

Google Earth images at two selected sites near the Taita Hills during 2014–2018 (please refer to Paper IV for details of this method). The space-for-time approach identifies the potential impacts of LCC between contrasting vegetation types that share similar environmental conditions (Duveiller, 2018).

Two methods were used to quantify the impacts of LCC on LST and decompose into radiative and non-radiative mechanisms. The first was the IBPM (Lee et al., 2011) and the second was the EBD approach (Luyssaert et al., 2014). Both metrics are based on surface energy balance equations.

The first method (IBPM), which was applied regionally in the HoA (Paper II), breaks down the contribution of biophysical changes to the total LST change (ΔTs) into radiative (albedo; first term on the right side of Eq. 3) and non-radiative (ET and SR; second term in the right side of Eq. 3) components:

$$\Delta T_s = (\lambda o \times \Delta S) / (1+f)) + (-\lambda o \times R_n \times \Delta f) / (1+f)^2 \quad (3)$$

where λo is the 2001–2013 monthly mean temperature sensitivity from the longwave radiation feedback (K $(W\ m^{-2})^{-1}$); ΔS is the net shortwave radiation change; Rn is the monthly mean net radiation; and f is the monthly mean energy redistribution factor and Δf is its change. The f was calculated from surface and air temperatures, net radiation, and ground heat flux (G) with Eq. 4 by rearranging the supplementary Eq. S7 reported in Lee et al., (2011). In data-scarce regions, the computation of f using Eq. 4 has an extra advantage of avoiding the difficulty and associated uncertainty in the estimation of an aerodynamic resistance term in its original formulation (Bright et al., 2016).

$$f = \lambda o / (Ts - Ta) (R_n^* - G) - 1 \quad (4)$$

where λo, R*n ≈ Rn, and G are as described in Eq.1; and Ts and Ta are surface and air temperature, respectively. Rn was estimated from the incoming shortwave radiation (SWin), total shortwave black-sky albedo (α), the Stefan–Boltzmann constant (σ), air emissivity (ea), surface emissivity (es), and Ta (Cleugh et al., 2007):

$$R_n = SW_{in} (1-\alpha) + \sigma * (e_a - e_s) * Ta^4 \quad (5)$$

$$e_a = 1 - 0.261 * \exp(-7.77 * 10^{-4} * Ta^2) \quad (6)$$

G was computed from the G/Rn ratio (Bastiaanssen, 2000) as in Eq. 7, which was derived from Ts, α, and the normalized vegetation index (NDVI = NIR–R / NIR+R, where NIR is near infrared reflectance and R is red reflectance). The NDVI was estimated from MODIS BRDF after the effects of sun-sensor geometry artifacts on the surface reflectance were corrected by fixing the sun angle at 45° and sensor view at nadir (Schaaf et al., 2002).

$$G/R_n = (Ts - 273.15) (0.0038 + 0.0074*\alpha) (1 - 0.98 * NDVI^4) \quad (7)$$

Furthermore, to check the robustness of the IBPM model, the calculated LST (ΔTs) was compared with observed LST changes (ΔT's) from MODIS 11A2. For this, the impacts of background climate signals on the ΔT's were identified using adjacent stable pixels within a 9 x 9 km window from a target pixel and removed from the analysis (please refer to Paper II for details of the method). Then, the corrected ΔT's were compared with the ΔTs in a scatterplot.

In the EBD approaches, which were applied locally at selected sites in Paper IV, the surface temperature change was decomposed into each of the energy balance components, derived from first-order derivatives of surface energy balance (Eq. 8; Luyssaert, 2014). This approach is often used in the comparison of adjacent areas with different land cover or management types (Luyssaert et al., 2014; Duveiller et al., 2018).

$$\Delta Ts = (-R_{si} \Delta\alpha + (1 - \alpha) \Delta Rsi + \Delta Rli - \Delta\lambda E - \Delta H - \Delta G - \sigma Ts^4 * \Delta\varepsilon) / (4\varepsilon\sigma Ts^3) \quad (8)$$

where Δα is the albedo change; ΔRsi is the incoming shortwave radiation change; ΔRli is the incoming longwave radiation change; ΔλE is the LE flux change; ΔH is the sensible heat flux change; ΔG is the ground heat flux change; and ΔƐ is the emissivity change. All changes in these parameters were computed within a 300 × 300 m grid applying the space-for-time approach (Blois et al., 2013; Duveiller et al., 2018). Here, the calculated ΔTs was also compared with the observed ΔT's, which was extracted from the Landsat 8 thermal band applying a single-channel algorithm (Jimenez-Munoz et al., 2009). The topographic effect was corrected from ΔT's using a standard lapse rate of 0.0065°C $m^{-1}$ prior to comparison.

## 4.4 Analysing energy exchange and land surface temperature anomalies during precipitation extremes

Pixels affected by precipitation extremes were identified using World Meteorological Organization (WMO) SPI value classifications (WMO, 2012) for the major rainfall seasons in the region (MAM = March, April, May; and OND = October, November, December). Both drought (SPI < −1) and extreme wet (SPI > 1) events were considered in the analysis for four major vegetation classes in the region (shrubland, grassland, savanna, and forest).

To measure how different intensities of precipitation extremes affect spectral albedo (VIS, NIR, and SW broadband albedo), absolute anomalies for each WMO SPI bin were estimated during 2001–2016. To do this, both albedo and SPI data were first detrended to avoid spurious correlations; pixels affected by anthropogenic changes (e.g., land cover changes) were excluded from our analysis by selecting only stable pixels from natural vegetation following the approach in subsection 4.3; and average absolute anomalies were calculated for each vegetation class. The effect of albedo change on the energy balance was computed from its shortwave surface radiative forcing during drought and extreme wet events.

For the same pixels identified in the previous step, the energy balance terms were computed as follows. Net radiation (Rn) was calculated using the CERES EBAF surface product:

$$Rn = (SW_{in} - SW_{out}) + (LW_{in} - LW_{out}) \quad (9)$$

where SWin and SWout are the downwelling and upwelling SW radiation flux; and LWin and LWout are downwelling and upwelling LW radiation flux. Latent heat flux (ʎE in W $m^{-2}$) was retrieved using Eqs. 10 and 11 (Dingman, 2015):

$$ʎE = \rho_w * ʎv * ET \quad (10)$$

$$ʎv = 2.495 - (2.36 * 10^{-3}) * (Tair - 273) \quad (11)$$

where ρw is the density of water (1000 kg $m^{-3}$); λv is the heat of vaporization (MJ $kg^{-1}$); ET is GLEAM 3.2a ET data (mm $day^{-1}$); and Tair is air temperature (K) from MERRA-2. G was estimated by multiplying G/Rn (Eq. 7) by Rn (Eq. 9). The H flux was estimated as a residual of the energy balance equation from Rn, ʎE, and G:

$$H = Rn - (ʎE + G) \quad (12)$$

Absolute anomalies for each of the radiation energy fluxes (ΔRn, SWin, SWout, LWin, and LWout), turbulent energy fluxes (ΔH and ʎE), and vegetation indices (NDVI and LAI from the SPOT VEGETATION and PROBA-V sensors) were computed during drought and extreme wet events. Finally, the impacts of precipitation extremes on albedo, energy exchange, and LST were assessed statistically using quantile regression, because it is robust against outliers, does not make assumptions about the distribution of data, and estimates the response of a variable in all parts of its data distribution (Koenker, 2005).

# 5 Results

## 5.1 Effects of rainfall-vegetation interaction on land surface temperature

The results of Paper I revealed a strong rainfall–vegetation relationship and impact on LST seasonality (Figure 4a–c). Of the total vegetated area of the HoA, 78% showed strong and positive correlations ($r > 0.7$; $P < 0.05$) between rainfall and vegetation. Furthermore, vegetation seasonal growth followed rainfall modality patterns in 81% of the region (Figure 4b). This meant that vegetation showed one peak (two peak) greening in areas that received unimodal (bimodal) rainfall, except along the unimodal–bimodal transition zones in the western humid parts of the region. In both unimodal and bimodal areas, where rainfall–vegetation interaction was very strong ($r \geq 0.8$), the LST exhibited a negative seasonal relationship with vegetation patterns across ecoregions (forest, grassland, and shrubland) and rainfall modalities (Figure 4c). Regression analysis showed that LST seasonal patterns (dependent variable) were negatively related to EVI patterns (predictor variable). The relationship was significant ($P < 0.05$) across biomes except in scarcely vegetated arid areas (Paper I).

However, during forest loss events analyzed samples from unimodal and bimodal areas (in Ethiopia and Kenya) showed that LST changes had different seasonal patterns between dry and wet periods (Figure 5, Paper I). Following forest loss, although an overall average increment of up to 1.8°C was observed, the increment exhibited an inconsistent pattern across seasons. In dry periods, the increase was relatively strong (up to 3°C on average) and consistent, whereas in wet seasons it fluctuated. This wet period fluctuation was associated with the effects of rainfall through improved soil moisture availability, ET, and greening of the surface that replaced forest (cropland and pastures), as was observed in the increased EVI during this period (Figure 5a, c, e).

Analyses of rainfall, vegetation, and LST during drought events further demonstrated the importance of vegetation vigor (greenness) in modulating LST anomalies (Paper I). For instance, during severe drought, LST anomalies were higher (1.57σ on average) when vegetation greenness was considerably affected (EVI anomaly $< -2\sigma$), whereas in areas where vegetation greenness was maintained, the LST anomaly was highly minimized (0.14 to 0.34σ) or even avoided (–0.7σ) on average.

## 5.2 Climatic impacts of vegetation seasonality across biomes

Growing-period albedo dynamics displayed contrasting patterns between forest and savanna on the one hand, and shrubland and grassland on the other (Paper II). Albedo increased by 8% in forest and 27% in savanna, and caused reductions in the available energy of $-2.47$ W m$^{-2}$ and $-10$ W m$^{-2}$, respectively. By contrast, albedo decreased in grassland and shrubland by 18% and 10%, respectively, which raised the available energy by 7.11 W m$^{-2}$ and 5.04 W m$^{-2}$.

However, albedo dynamics had minor impacts on the seasonality of LST (Paper II). For instance, the multiple regression coefficients of albedo exhibited considerable variations in sign and magnitude, and had a nonsignificant ($P>0.05$) relationship with LST (dependent variable) for most parts of the region. By contrast, ET had a significant ($P < 0.05$) and consistently negative relationship with LST across biomes. The results showed that regardless of the sign and magnitude of albedo changes, LST seasonality

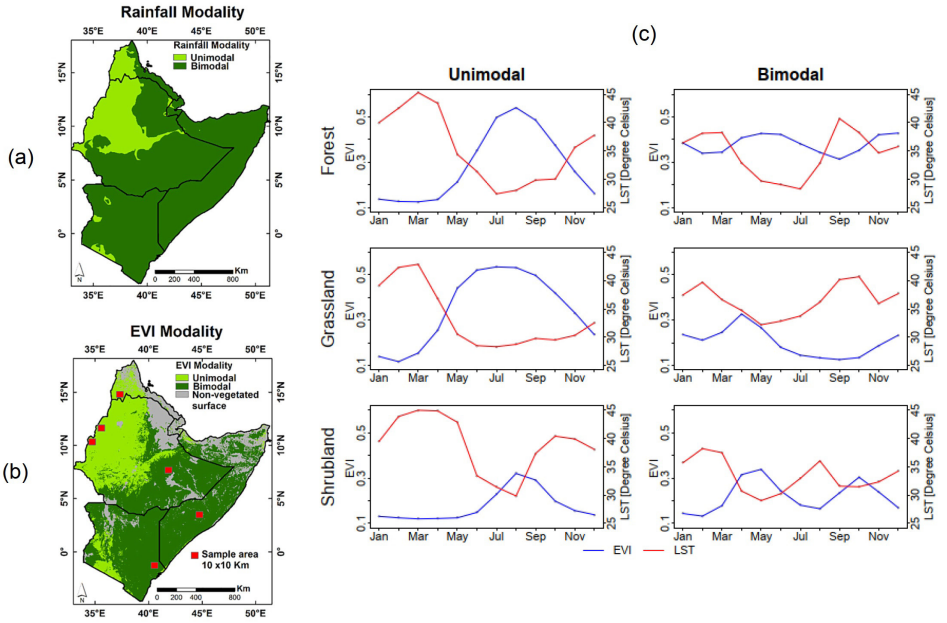


Figure 4. (a) Rainfall modality patterns, (b) vegetation seasonal modality patterns, and (c) seasonality of land surface temperature (LST) and enhanced vegetation index (EVI) across biomes (forest, grassland, and shrubland) and rainfall modality patterns.

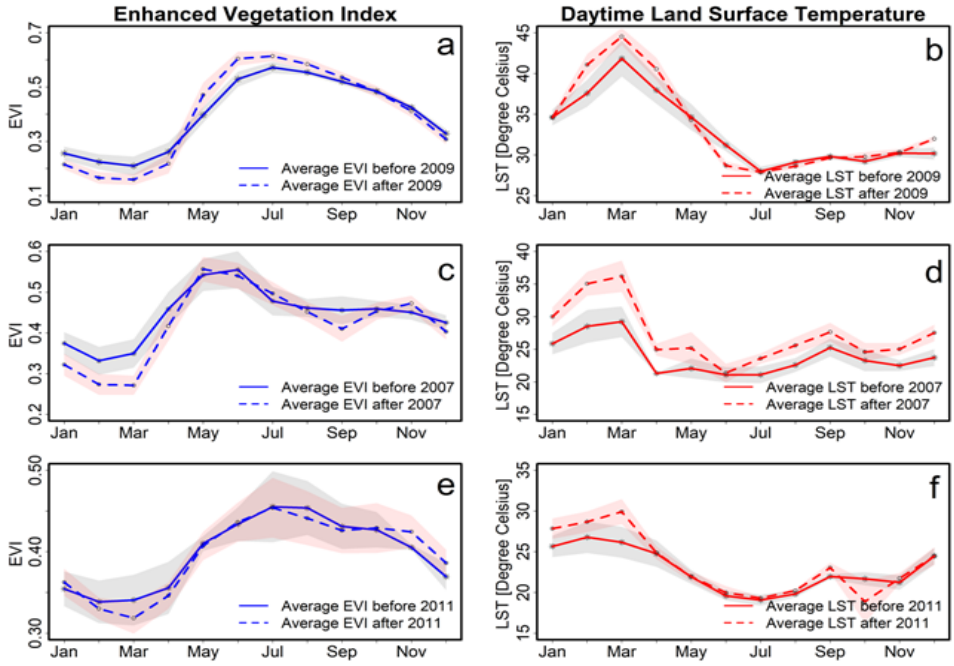


Figure 5. Dry- and wet-period seasonality of enhanced vegetation index (EVI) and land surface temperature (LST) before and after forest loss at three sites in the study area: (a,b) Abobo, (c,d) Shakiso, and (e,f) Kapcherop. Shaded area indicates ± standard deviation.

was mainly driven by ET changes in the region.

## 5.3 Radiative and non-radiative impacts of land cover change on land surface temperature

Our regional analysis at a 1-km resolution, which was based on the actual conversion of multiple land cover types durng 2001–2013 (Figure 6a), revealed a considerable impact of woody vegetation conversion (Paper II). Albedo change from all conversion classes (forest-to-cropland, savanna-to-grassland, grassland-to-shrubland, shrubland-to-grassland, savanna-to-mixed cropland/vegetation, and savanna-to-cropland) generated an annual average regional surface radiative forcing of −0.03 ± 0.02 W $m^{-2}$. The albedo changes in forest-to-cropland and savanna-to-grassland conversions generated the largest mean albedo change across seasons compared with other conversion classes. However, the contributions to the net LST change from these radiative changes were minor (0.12 K and 0.09K) on average and were highly outweighed by the nonradiative mechanisms (ET and SR), generating a maximum average warming of 1.2 K in forest-to-cropland and 0.23 K in savanna-to-grassland conversions (Figure 6b). The warming from these conversion classes was consistent across seasons, whereas other conversion classes showed inconsistent results.

Comparison of the observed (MODIS) and calculated (IBPM) LST differences across seasons revealed a moderate agreement ($r^2$ = 0.77) in the dry season (December–February), whereas wet seasons showed relatively larger uncertainties ($r^2$ ranges from 0.5 to 0.62). When the magnitude of uncertainties compared among conversion classes, forest-to-cropland and savanna-to-grassland conversions had the smallest uncertainties.

A large-scale analysis of bushland (Acacia-Commiphora)-to-cropland conversion in two sites (Mwatate and Ndome) at 300-m resolution revealed its important role in the local climate (Paper IV; Figure 6c and d). The conversion of bushland to cropland led to an increase in albedo in the VIS, NIR, and SW ranges. Locally, the increase in albedo reduced the available SW energy at the surface by up to 6.02 W $m^{-2}$, which in turn induced an average cooling of 0.8 K. The cooling impact from an increase in SW albedo was highly outweighed (approx. 5 times) by the reduction of LE flux, causing net warming of 1.75 K on average (Figure 6d). This magnitude was comparable with the average maximum local forest loss impact reported (1.8 K) in the region (Paper I). Moreover, a comparison of observed ΔLST (Landsat 8) and calculated (EBD) ΔLST showed good agreement ($r^2$ = 0.95 for Mwatate and $r^2$ = 0.89 for Ndome).

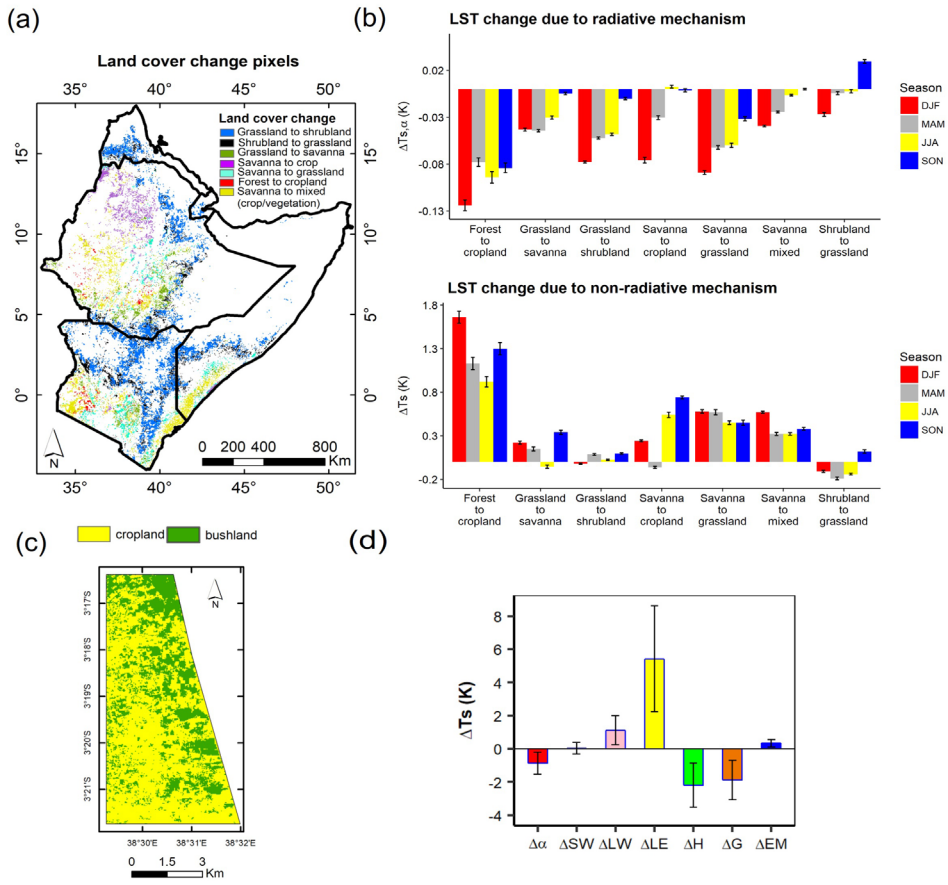


Figure 6. (a) Land cover change across the Horn of Africa between 2001 and 2013; (b) average surface temperature change (ΔTs) caused by radiative (albedo) and non-radiative (ET and SR) mechanisms from multiple land cover conversions across seasons (DJF = December, January, February; MAM = March, April, May; SON = September, October, November); the error bar shows the 95% confidence interval of the mean; (c) distribution of cropland and bushland derived from RapidEye imagery at Ndome, southern Kenya; (d) potential ΔTs (mean ± SD) due to changes in radiation and energy balance terms (α = albedo, SW = incoming shortwave radiation, LW = incoming longwave radiation, LE = latent heat flux, ΔH = sensible heat flux, G = ground heat flux, EM = emissivity) following bushland-to-cropland conversion at Ndome.

## 5.4 Effects of precipitation extremes on surface energy balance and land surface temperature

Analysis of the impact of precipitation extremes on climate revealed different responses across biomes during 2001–2016 (Paper III). Albedo changes in the VIS and NIR ranges were opposite and cancelled each other, and thus limited the changes in the total SW in forest ($P > 0.05$) and savanna ($P < 0.05$) across seasons (March–May and October–December). Contrary to this pattern, VIS and NIR albedo increased during drought events in shrubland in both seasons, as well as during March–May in grassland. The resulting SW albedo changes

were larger in magnitude and significant ($P < 0.01$) in shrubland and grassland. However, regardless of the different spectral albedo patterns observed across biomes, the albedo changes in the visible range were dominant in the region.

When this study assessed the impacts of albedo changes on the regional SW radiation balance, the results indicated that the drought event regional SW radiative forcing (−0.64 W $m^{-2}$ ± SD 0.11) was approximately twice that of extreme wet events (0.33 W m−2 ± SD 0.09) (Figure 7a and b). Nonetheless, the magnitudes of the radiative forcing were too small to affect the land–atmosphere coupling in the region as well as the LST.

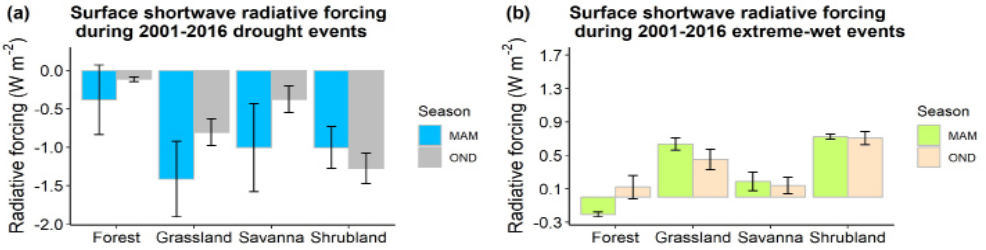


Figure 7. Surface shortwave radiative forcing (mean ± SD) during drought and extreme wet events across biomes (forest, grassland, savanna, and shrubland) and seasons (MAM = March, April, May; OND = October, November, December) during 2001–2016.

Furthermore, precipitation extremes had a statistically significant ($P < 0.01$) impact on energy exchange anomalies across biomes (grassland, shrubland, and savanna) except in forest (Paper III). The energy exchange anomalies during drought and extreme wet events were opposite in sign, which meant that during drought, the latent heat flux anomaly (ΔLE) reduced strongly, whereas the sensible heat flux anomaly (ΔH) increased by a comparable magnitude. The reverse patterns occurred during extreme wet events. Forest displayed the smallest ΔLE during both drought (−2.69 W $m^{-2}$, SD 0.72 in OND) and extreme wet events (−1.64 W $m^{-2}$, SD 3.73 in OND), whereas grassland had the strongest ΔLE during drought (i.e., decreased by −28.10 W $m^{-2}$, SD 4.86 in OND) and extreme wet events (i.e., increased by 24.51 W $m^{-2}$, SD 8.87 in MAM).

During precipitation extremes, grassland displayed the strongest ΔLST while forest displayed the weakest (Table 2). Nonetheless, ΔLST was significant ($P < 0.01$) across biomes (forest, savanna, grassland, and shrubland). Overall, the results of the difference between extreme wet and drought event anomalies (in energy exchange, LST, and vegetation index) showed that forests were resilient, whereas grasslands were the most sensitive to precipitation extremes.

Table 2. Summary of extreme wet minus drought-period anomalies of surface energy balance terms, LST, and vegetation indices during 2001–2016 March–May and October–December; the range of values indicates variation between two seasons.

| Extreme wet minus drought (Difference) | | | | | | | | |
|---|---|---|---|---|---|---|---|---|
| IGBP Vegetation type | ΔRn ($W\ m^{-2}$) | ΔLE ($W\ m^{-2}$) | ΔH ($W\ m^{-2}$) | ΔSWin ($W\ m^{-2}$) | ΔLWout ($W\ m^{-2}$) | ΔLAI ($W\ m^{-2}$) | ΔEVI | ΔLST (K) |
| Forest | 1–2 | 1–26 | −0.1 to −24 | −14 | −6 to −9 | 0.3–0.5 | 0.02–0.06 | −1 to −2 |
| Savanna | 2–3 | 21–42 | −19 to −40 | −12 to −16 | −8 to −11 | 0.4–0.5 | 0.05–0.08 | −3 to −4 |
| Shrubland | 4–7 | 35–38 | −31 | −13 to −15 | −11 to −12 | 0.2–0.4 | 0.06–0.08 | −3 |
| Grassland | 5–7 | 46–49 | −41 to −42 | −13 to −15 | −13 | 0.5–0.6 | 0.09–0.1 | −4 |

Rn = net radiation; LE = latent heat flux; H = sensible heat flux; SWin = incoming shortwave radiation; LWout = outgoing longwave radiation; leaf area index (LAI); enhanced vegetation index (EVI); land surface temperature (LST); and IGBP = International Geosphere-Biosphere Programme.

# 6 Discussion

Understanding climate sensitivity to vegetation dynamics across different ecosystems is crucial for evaluating climate regulation services as well as setting effective land use plans and mitigation strategies. In the EA, despite the occurrence of multiple factors causing vegetation dynamics (e.g., multiple growing periods, rapid agricultural expansion, and recurrent drought events), the biophysical impacts on LST had not been quantified and were poorly understood at a regional (local) scale across biomes and seasons. The results of this thesis, which are briefly discussed below, provide evidence for the impacts of vegetation dynamics on LST and broaden our understanding of the underlying biophysical changes driving LST.

## 6.1 Impacts of seasonal vegetation dynamics on land surface temperature

Vegetation had strong control over the seasonality of LST across ecoregions and rainfall modality patterns (Paper I), mainly through nonradiative mechanisms (Paper II). This meant that the seasonality of LST was negatively related to vegetation greening patterns across biomes and rainfall modality patterns except in scarcely vegetated arid areas (Paper I). The underlying biophysical changes driving seasonal LST dynamics were dominated by ET and SR, whereas albedo only had a minor influence (Paper II).

Relevant in situ studies in the tropics and beyond have observed concomitant increases in albedo in taller vegetation (deciduous forest and savanna) and decreases in albedo in shorter vegetation (grassland and shrubland) during growing period (Samain et al., 2006; Ryu et al., 2008; Hollinger et al., 2010). The cause behind the decline in the growing-period albedo of shorter vegetation can be explained by the dominant influence of the wet background soil albedo and lower reflectance of green

grasses and shrubs compared with dry-season albedo (Samain et al., 2006; Hollinger et al., 2010). Regardless of the albedo patterns, LST dynamics during growing periods were strongly affected by ET. For instance, the albedo decrease (warming effect) in shorter vegetation weakly counterbalanced the cooling effect from an increase in ET, leading to a reduction in LST in the growing period (Paper II).

This result provides new insights into the underlying biophysical factors driving LST seasonality across biomes. In particular, under a projected increase in temperature and drought frequency (Nicholson, 2017; Allen et al., 2018), shorter growing periods can be expected. This might increase or reverse the growing-period albedo pattern in grassland and shrubland ecosystems (Paper III) as well as affect the annual energy balance. However, further studies are required to explore the extent to which a shift in vegetation growing period or phenology alters the land–atmosphere energy exchange and LST. Specially, in response to recurrent drought in the region, whether this shift can accelerate or reduce rates of climate change requires additional investigation.

## 6.2 Impacts of land cover change on land surface temperature

The multiscale observation of the impacts of LCC on the climate showed that LST changes were mainly driven by nonradiative mechanisms (ET and SR) (Paper II and IV). Radiative (albedo) changes were highly outweighed by ET and played only a minor role. In a decreasing order of magnitude, the conversion of forests, bushland, and savanna to cropland/grassland generates stronger LST warming than other conversion classes. Compared with cropland/grassland, woody vegetation (forest, bushland, , and savanna) has higher ET and SR efficiency through their deep rooting system and LAI; hence, their conversion to cropland/grassland can cause reductions in ET and SR, leading to surface warming in the tropics (Jackson et al., 1997; Miranda et al., 1997; Bonan, 2008; Davin and De Noblet-Ducoudre, 2010). However, the warming impact (e.g., during forest loss) was stronger during the dry season (Paper I). Locally, wet-period warming fluctuated (Paper I) because of enhanced greening, soil moisture/precipitation, ET, cloud cover, and reduction of insolation.

The results obtained from regional level assessments in forest and savanna conversions conducted for this thesis agreed with previous global (modeling and observational) studies in the tropics (Davin and De Noblet-Ducoudre, 2010; Alkama and Cescatti, 2016; Li et al., 2016; Bright et al., 2017; Duveiller et al., 2018; Hoffman and Jackson et al., 2000). The impacts of bushland conversions, which were not identified in such studies, were revealed using a small-scale biophysical study (Paper IV). In large-scale studies, the limitations on resolving fragmented patches of land conversion and the occurrence of cropland mixed with other vegetation classes suggest the importance of small-scale biophysical studies for better quantification of anthropogenic climate impacts of LCC in the region.

These results (Paper II) can be used to warn of the impacts on regional radiation balance and surface warming generated from multiple LCCs in the region. Furthermore, the regional radiative forcing can provide information for computing the contribution to the global energy balance (Paper II) through its impact at the TOA level (Bright, 2015). Moreover, the methods (Paper II) can contribute to the development of regional level monitoring,

verification, and reporting of the biophysical impacts of multiple LCCs, as has been done for its biogeochemical counterparts, for example through REDD+ ( Reducing emissions from deforestation and forest degradation and the role of conservation, sustainable management of forests and enhancement of forest carbon stocks in developing countries).

Furthermore, the results of the biophysical effect of LCCs can be used to assess the performance of land surface models. Previous model comparison studies have shown conflicting results for the sign of biophysical effects of LCCs (Pitman et al., 2009; Devaraju et al., 2015). In addition, isolating and detecting local LCC signals from nonlocal climate signals is difficult because of the coarse resolution in models as well as uncertainties (Pitman et al., 2009; Li et al., 2015a; Duveillor et al., 2018). Thus, the observation-based results presented in this thesis can help to verify the performance of land surface models in simulating the biophysical effects of LCCs in the region.

Some additional considerations on the interpretation of the results are necessary. The impacts of land conversion addressed in Paper II, which are based on data at a 1-km$^2$ resolution, could contain incorrectly classified pixels associated with the inherent limitations in the accuracy of the LCC product used (approx. 75%). Furthermore, quantification of LST changes using the IBPM method had moderate agreement in wet season, unlike the good agreement obtained in dry season, and thus must be used carefully. Additional investigations are required to improve the parametrization and performance of this method, particularly in the wet season. In this regard, the future availability of flux tower data across different biomes will help in the validation of local- and regional-scale observation-based biophysical metrics in the region.

## 6.3 Land surface temperature change during precipitation extremes

During precipitation extremes, LST sensitivities varied across ecosystems. Vegetation greening had a strong influence on regulating the impact of droughts on temperature anomalies. The highest LST anomalies were displayed in grasslands, followed by savannas and shrublands. Forests were the most resilient vegetation type to precipitation extremes (Paper III). These results are in line with a previous study that reported stronger energy exchange and warming over grasslands than over forests during a European drought (Teuling et al, 2010). Moreover, regardless of drought intensity (from mild to severe), areas that maintained vegetation greenness were able to minimize or avoid surface warming (Paper I).

The underlying biophysical mechanisms driving LST anomalies were mostly dominated by LE flux changes, whereas the impact of SW albedo changes was minor. Comparing spectral albedo changes during droughts revealed contrasting VIS and NIR albedo in forest and savanna. This result agreed with relevant studies conducted during European drought (Teuling et al., 2008; Sütterlin et al., 2016). However, the VIS and NIR albedo increases in shrubland and grassland during drought events were new findings in arid regions. In these vegetation types, the increase in NIR albedo together with VIS can be explained by the dominant NIR albedo increase from a bare soil fraction (approx. 60%) that outweighed the NIR decrease from stressed vegetation

cover fraction (~ 40%) during drought, as evidenced in Paper III.

Under the increasing trend of extreme events in the region, the sensitivity of LST to precipitation extremes across ecosystems in the EA provides a crucial benchmark for planning mitigation strategies. Forest preservation and afforestation activities can provide vital climate regulatory services during droughts. The savanna ecosystem also deserves strong attention given its coverage being larger than that of forest and it being mixed with grasslands, which are strongly sensitive to droughts. Thus, clearing of savannas for grazing land could exacerbate surface warming during droughts in the region, and such activities need to consider their environmental impacts.

Finally, the results of this thesis are vital for the design of effective land use policies and climate change mitigation strategies in East Africa. With agricultural expansion increasing to meet the growing demand for food production, an optimized climate-smart land use policy that can efficiently utilize the land without inducing further warming is required. In this respect, land use policies that account for LST sensitivity to multiple LCC classes and climate extremes can support mitigation efforts (e.g., afforestation or reforestation and the preservation of woody cover). Furthermore, because the biophysical impacts of LCCs are stronger in the source area of perturbations (Bright et al., 2015; IPCC, 2019), their inclusion in local land use plans could directly benefit the region.

Current mitigation efforts are mainly focused on forest and the reduction of CO2 emissions; however, the results of this thesis demonstrated that other classes of woody land cover such as bushlands (Acacia-Commiphora) also require attention from a biophysical perspective, given their important regulating effect on the LST. Moreover, with a projected increase in temperature faster than the global average, evaluation of mitigation efforts (e.g., REDD+) will benefit from considering the relative contribution of individual ecosystems to climate regulation services in the region. For this, the surface cooling benefit through biophysical processes (enhanced ET and SR) needs to be considered along with biogeochemical processes (i.e., the reduction of CO2 emissions). In particular, because the net impact of these two processes might not counteract in tropical regions (IPCC, 2019), larger cooling benefits can be obtained from mitigation efforts.

# 7 Conclusions

This thesis assessed the climatic impacts of vegetation dynamics in Eastern Africa. Comprehensive analysis was performed across biomes, during seasonal growing cycles, LCCs, and precipitation extremes. Regional-and local-level biophysical effects were evaluated mainly using satellite observation data. The main conclusions of the thesis are summarized as follows.

i. **The role of seasonal vegetation–rainfall dynamics on land surface temperature patterns**

The seasonal vegetation greening cycle had an inverse relationship with LST patterns. This result was consistent across biomes and rainfall modality except in scarcely vegetated arid areas. The biophysical mechanism driving LST temporal dynamics was dominated by ET seasonality. The impacts of albedo were too small and largely nonsignificant across space regardless of the increase (deciduous forest and savanna) or decrease (grassland and shrubland) in albedo in the growing period.

**ii. The impacts of multiple land cover change on land surface temperature**

Woody vegetation loss (forest, bushland, and savanna) induced stronger surface warming. However, the increase was bigger in the dry season, and locally, LST could fluctuate (e.g., after forest loss) from enhanced vegetation greening and rainfall during the wet season. In other LCCs, the assessment of climatic impacts carried larger uncertainties, mainly because of the occurrence of mixed vegetation classes at 1-km resolution. Therefore, future studies will benefit from the use of high-resolution imagery, particularly in the case of bushland (Acacia-Commiphora) conversion.

iii. **The relative contribution of radiative and non-radiative mechanisms to land surface temperature changes during land cover conversion**

Non-radiative mechanisms (ET and SR) had strong contributions and control over LST changes during woody vegetation loss compared with radiative mechanisms (albedo). In forest-to-cropland conversion, the surface warming from reductions of ET and SR was up to 10 times stronger than the cooling effect from albedo increases. Similarly, in bushland-to-cropland transition, latent heat flux reduction alone generated surface warming up to five times stronger than the albedo cooling effect.

**iv. Energy exchange and land surface temperature sensitivity during precipitation extremes across biomes**

During precipitation extremes, LE flux anomalies dominated the energy exchange and had strong impacts in driving LST anomalies across biomes. During drought, the SW albedo increase in shorter vegetation (shrubland and grassland) was stronger than that in woody vegetation (forest and savanna). However, the albedo increase was too small to counterbalance the surface warming from the strong LE flux decline in both vegetation classes. Much of the available energy was used to warm the surface and increase LST and sensible heat anomalies. In comparison, LST in grasslands showed stronger surface warming and sensitivity to droughts, followed by savanna, whereas forests exhibited the smallest changes in LST and were relatively resilient. The LST pattern was regulated by the status of vegetation vigor (greening). In the areas where vegetation greenness was maintained, surface warming was highly minimized during mild to severe droughts.

Overall, the non-radiative mechanisms were shown to dominate the biophysical climatic impacts of vegetation dynamics through their strong influence on LST changes in the Eastern Africa.

## References


Adeyewa, Z. D., and Nakamura, K. (2003). Validation of TRMM radar rainfall data over major climatic regions in Africa. J. Appl. Meteor., 42, 331–347. https://doi.org/10.1175/1520-0450(2003)042<0331:VOTRRD>2.0.CO;2

Alkama, R. and Cescatti, A. (2016). Biophysical climate impacts of recent changes in global forest cover. Science, 351(6273), 600–604. https://doi.org/10.1126/science.aac8083

Allen, M.R., Dube, O.P., Solecki, W. F., Aragon-Durand, Cramer, W., Humphreys, S … Zickfeld, K. (2018). An IPCC Special Report on the impacts of global warming of 1.5°C above pre-industrial levels and related global greenhouse gas emission pathways, in the context of strengthening the global response to the threat of climate change, sustainable development, and efforts to eradicate poverty. In Press.

Anderegg, W. R. L., Trugman, A. T., Bowling, D. R., Salvucci, G., & Tuttle, S. E. (2019). Plant functional traits and climate influence drought intensification and land–atmosphere feedbacks. Proceedings of the National Academy of Sciences, 201904747. https://doi.org/10.1073/pnas.1904747116

Arnfield, A.J. (2003). Two decades of urban climate research: a review of turbulence, exchanges of energy and water, and the urban heat island. International Journal of Climatology 23: 1–26. http://dx.doi.org/10.1002/joc.859

Avila F. B., Pitman A. J., Donat, M. G., Alexander, L.V., Abramowitz, G. (2012). Climate model simulated changes in temperature extremes due to land cover change. Journal of Geophysical Research 117: D04108. DOI: 10.1029/2011JD016382

Baldocchi, D. D., Xu, L., & Kiang, N. (2004). How plant functional-type, weather, seasonal drought, and soil physical properties alter water and energy fluxes of an oak-grass savanna and an annual grassland. Agricultural and Forest Meteorology, 123(1–2), 13–39. https://doi.org/10.1016/j.agrformet.2003.11.006

Betts, R. A. (2000). Offset of the potential carbon sink from boreal forestation by decreases in surface albedo Nature, 408, 187–90. https://doi.org/10.1038/35041545

Blois, J. L., Williams, J. W., Fitzpatrick, M. C., Jackson, S. T., & Ferrier, S. (2013). Space can substitute for time in predicting climate-change effects on biodiversity. Proceeding of the National Academy of Sciences of the United States of America, 110(23), 9374–9379, https://doi.org/10.5061/dryad.d5f1r

Boisier J. P., De Noblet-Ducoudré, N., Pitman, A.J., Cruz, F.T., Delire, C., Van Den Hurk, B.J.J.M and Voldoire, A. (2012). Attributing the impacts of land-cover changes in temperate regions on surface temperature and heat fluxes to specific causes: results from the first LUCID set of simulations J.Geophys. Res. Atmos. 117 1–16. https://doi.org/10.1029/2011JD017106

Bonan, G. B. (2008). Forests and Climate Change: Forcings, Feedbacks, and the Climate Benefits of Forests. Science, 320(5882), 1444–1449. http://dx.doi.org/10.1126/science.1155121

Bonan, G.B. (2015). Ecological Climatology: Concepts and Applications. Cambridge: Cambridge University Press. doi:10.1017/CBO9781107339200

Bouvet, A., Mermoz, S., Le Toan, T., Villard, L., Mathieu, R., Naidoo, L., & Asner, G. P. (2018). An above-ground biomass map of African savannahs and woodlands at 25 m resolution derived from ALOS PALSAR. Remote Sensing of Environment, 206(November 2017), 156–173. https://doi.org/10.1016/j.rse.2017.12.030

Bright, R. M. (2015). Metrics for biogeophysical climate forcings from land

use and land cover changes and their inclusion in life cycle assessment: A critical review. Environmental Science and Technology, 49(6), 3291–3303. https://doi.org/10.1021/es505465t

Bright, R. M., Zhao, K., Jackson, R. B., Cherubini, F. (2015). Quantifying surface albedo and other direct biogeophysical climate forcings of forestry activities. Global Change Biology, 3246–3266. https://doi.org/10.1111/gcb.12951

Bright, R. M., Davin, E. L., O'Halloran, T. L., Pongratz, J., Zhao, K., & Cescatti, A. (2017). Local surface temperature response to land cover and management change driven by non-radiative processes. Nature Climate Change, 7(296), Forthcoming. https://doi.org/10.1038/nclimate3250

Brink, A. B., & Eva, H. D. (2009). Monitoring 25 years of land cover change dynamics in Africa: A sample based remote sensing approach. Applied Geography, 29(4), 501–512. https://doi.org/10.1016/j.apgeog.2008.10.004

Brink, A. B., Bodart, C., Brodsky, L., Defourney, P., Ernst, C., Donney, F., … Tuckova, K. (2014). Anthropogenic pressure in East Africa-Monitoring 20 years of land cover changes by means of medium resolution satellite data. International Journal of Applied Earth Observation and Geoinformation, 28(1), 60–69. https://doi.org/10.1016/j.jag.2013.11.006

Camberlin, P., Martiny, N., Philippon, N., & Richard, Y. (2007). Determinants of the interannual relationships between remote sensed photosynthetic activity and rainfall in tropical Africa. Remote Sensing of Environment, 106(2), 199–216. https://doi.org/10.1016/j.rse.2006.08.009

Campbell, G.S., Norman, J.M. (1998). An Introduction to Environmental Biophysics. Springer, New York, 286 pp.

Cao, Y., Zhang, W., & Wang, W. (2018). Evaluation of TRMM 3B43 data over the Yangtze River Delta of China. Scientific Reports, 8(1), 1–12. https://doi.org/10.1038/s41598-018-23603-z

Charney, J., P. H. Stone, and Quirk, W. J. (1975). Drought in the Sahara: A biogeophysical feedback mechanism, Science, 187, 434–435

Chen, L., & Dirmeyer, P. A. (2016). Adapting observationally based metrics of biogeophysical feedbacks from land cover/land use change to climate modeling. Environmental Research Letters, 11(3), 34002. https://doi.org/10.1088/1748-9326/11/3/034002

Claussen, M., Bathiany, S., Brovkin, V., Kleinen, T. (2013). Simulated climate–vegetation interaction in semi-arid regions affected by plant diversity. Nat. Geosci. 6 (11), 954–958. http://dx.doi.org/10.1038/ngeo1962.

Davin, E. L., and de Noblet-Ducoudre, N. (2010). Climatic impact of global-scale Deforestation: Radiative versus nonradiative processes. Journal of Climate, 23(1), 97–112. https://doi.org/10.1175/2009JCLI3102.1

Devaraju, N., Bala, G., & Nemani, R. (2015). Modelling the influence of land-use changes on biophysical and biochemical interactions at regional and global scales. Plant, Cell and Environment, 38(9), 1931–1946. https://doi.org/10.1111/pce.12488

Dickinson, R. E. (1983). Land surface processes and climate-surface albedos and energy balance. Advances in Geophysics, 25, 305–353.

Dingman, S. L. (2015). Physical hydrology (3rd ed.). Long Grove, IL: Waveland Press.

Duveiller, G., Hooker, J., & Cescatti, A. (2018). The mark of vegetation change on Earth's surface energy balance. Nature Communications, 9(1). https://doi.org/10.1038/s41467-017-02810-8

Evans, J. P., Meng, X., & Mccabe, M. F. (2012). Land surface albedo and vegetation feedbacks enhanced the millennium drought

in south-east Australia. Hydrol. Earth Syst. Sci., 21, 409–422, https://doi.org/10.5194/hess-21-409-2017

FAO, (2012). State of the world's forests. Food and Agriculture Organization of the United Nations, Rome, Italy, 60 pp.

Feddema, J. J., Oleson K.W., Bonan G. B., Mearns L. O., Buja, L. E., Meehl, G. A., Washington W. M. (2005). The Importance of land-cover change in simulating future climates. Science 310(5754), 1674–1678. DOI: 10.1126/science.1118160

Fischer, M. L., M. S. Torn, D. P. Billesbach, G. Doyle, B. Northup, and S. C. Biraud (2012). Carbon, water, and heat flux responses to experimental burning and drought in a tallgrass prairie, Agric. For. Meteorol., 166-167, 169–174. https://doi.org/10.1016/j.agrformet.2012.07.011

Fitzjarrald, D.R., Acevedo, O.C., Moore, K.E. (2001). Climatic consequences of leaf presence in the eastern United States. J. Climate 14, 598–614. https://doi.org/10.1175/1520-0442(2001)014<0598:CCOLPI>2.0.CO;2

Fleming, K., Awange, J., Kuhn, M., & Featherstone, W. (2011). Evaluating the TRMM 3B43 monthly precipitation products using gridded raingauge data over Australia. Australian Meteorological and Oceanographic Journal, 61(3), 171–184. https://doi.org/10.22499/2.6103.003

Foley, J. A., Coe M. T., Scheffer M, Wang G. (2003). Regime shifts in the Sahara and Sahel: interactions between ecological and climatic systems in Northern Africa. Ecosystems 6: 524–532. https://doi.org/10.1007/s10021-002-0227-0

Foley, J. A., et al. (2005) Global Consequences of Land Use. Science, 309, 570-574. http://dx.doi.org/10.1126/science.1111772

Folland, C. K., Palmer T. N., Parker, D. E. (1986). Sahel rainfall and worldwide sea temperatures, 1901–85. Nature 320:602–607. https://doi.org/10.1038/320602a0

Friedl, M., Sulla-Menashe, D. (2015). MCD12Q1 MODIS/Terra+Aqua Land Cover Type Yearly L3 Global 500m SIN Grid V006. NASA EOSDIS Land Processes DAAC, https://doi.org/10.5067/MODIS/MCD12Q1.006.

Funk, C., Hoell, A., Shukla, S., Blade, K., Liebmann, B., Roberts, J.B., Robertson, F.R., Husak, G. (2014). Predicting East African spring droughts using Pacific and Indian Ocean sea surface temperature indices. Hydrol. Earth Syst. Sci. 18, 4965–4978. https://doi.org/10.5194/hess-18-4965-2014

Funk, C. C., Senay, G., Aswaw, A., Verdin, J., Rowland, J., Korecha, D., Eilerts, G.,Michaelsen, J., Amer, S., Choularton, R. (2005). Recent drought tendencies in Ethiopia and equatorial-subtropical eastern Africa. In: Famine Early Warming System Network Special Report. US Agency for International Development.

Gates, D. M. (1965). Energy, plants, and ecology. Ecology. 46(1-2), 1–13. https://doi.org/10.2307/1935252

Hansen, M. C., Potapov, P. V., Moore, R., Hancher, M., Turubanova, S. A., Tyukavina, A., … Townshend, J. R. G. (2013). High-resolution global maps of 21st-century forest cover change. Science, 342(6160), 850–853. https://doi.org/10.1126/science.1244693

Hawinkel, P., Thiery, W., Lhermitte, S., Swinnen, E., Verbist, B., Orshoven, J.V., and B. Muys, B (2016). Vegetation response to precipitation variability in East Africa controlled by biogeographical factors. Journal of Geophysical Research: Biogeosciences, 121(9), 2422–2444. https://doi.org/10.1002/2016JG003436

Henderson-Sellers A, Dickinson RE, Durbidge TB, Kennedy PJ,McGuffie K, Pitman A. J. (1993). Tropical deforestation: modelling local- to regional-scale climate change. Journal of Geophysical Research 98: 7289–7315. https://doi.org/10.1029/92JD02830

Hirsch, A. L., Wilhelm, M., Davin, E. L., Thiery, W., & Seneviratne, S. I. (2017). Can climate-effective land management reduce regional warming? Journal of Geophysical Research, 122(4), 2269–2288. https://doi.org/10.1002/2016JD026125

Hoffman, W. A. and Jackson R. B. (2000). Vegetation-climate feedbacks in the conversion of tropical savanna to grassland. Journal of Climate 13:1593–1602. https://doi.org/10.1175/1520-0442(2000)013<1593:VCFITC>2.0.CO;2

Hollinger, D. Y., Ollinger, S. V., Richardson, A. D., Meyers, T. P., Dail, D. B., Martin, M. E., … Verma, S.V. (2010). Albedo estimates for land surface models and support for a new paradigm based on foliage nitrogen concentration. Global Change Biology, 16, 696–710. https://doi.org/10.1111/j.1365-2486.2009.02028.x

Huxman, T. E., Smith, M. D., Fay, P. A., Knapp, A. K., Shaw, M. R., … Williams, D. G. (2004). Convergence across biomes to a common rain-use efficiency. Nature, 429, 651–654. https://doi.org/10.1038/nature02561.

IPCC (2019). Climate Change and Land: an IPCC special report on climate change, desertification, land degradation, sustainable land management, food security, and greenhouse gas fluxes in terrestrial ecosystems. Chapter 2: Land-Climate Interactions. Final Government Distribution. https://www.ipcc.ch/srccl-report-download-page/, accessed on 15 August 2019.

Jackson, R. B., Mooney, H. A., and Schulze, E. D. (1997). A global budget for fine root biomass, surface area, and nutrient contents. Proc. Natl. Acad Sci., 94(14), 7362–7366. https://doi.org/10.1073/pnas.94.14.7362

Jimenez-Munoz, J. C., Cristobal, J., Sobrino, J. A., Sòria, G., Ninyerola, M., & Pons, X. (2009). Revision of the single-channel algorithm for land surface temperature retrieval from landsat thermal-infrared data. IEEE Transactions on Geoscience and Remote Sensing, 47(1), 339–349. https://doi.org/10.1109/TGRS.2008.2007125

Jin, M., Dickinson, R. E., and Vogelmann A. M. (1997). A comparison of CCM2/BATS skin temperature and surface-air temperature with satellite and surface observations. J. Clim. 10, 1505–1524. https://doi.org/10.1175/1520-0442(1997)010<1505:ACOCBS>2.0.CO;2

Jin, M., Dickinson, R. E., and Zhang, D. L. (2005). The footprint of urban areas on global climate as characterized by MODIS. J. Clim. 18, 1551–1565.

Jin, M., Dickinson, R. E., (2010). Land surface skin temperature climatology: benefitting from the strengths of satellite observations. Environ. Res. Lett. 5 (4), 44004. http://dx.doi.org/10.1088/1748-9326/5/4/044004.

Kerhoulas, L.P., Kolb, T.E., Hurteau, M.D. & Koch, G. W. (2013). Managing climate change adaptation in forests: a case study from the U.S. Southwest, J. Appl. Ecol., 50, 1311–1320, https://doi.org/10.1111/1365-2664.12139.

Koenker, R. (2005). Quantile Regression, Cambridge University Press, ISBN 0-521-60827-9.

Lawrence, P. J. and Chase, T. N. (2010). Investigating the climate impacts of global land cover change in the Community Climate System Model (CCSM). International Journal of Climatology 30: 2066–2087.

Lee, E., Chase, T. N., and Rajagopalan, B. (2008). Highly improved predictive skill in the forecasting of the East Asian summer monsoon. Water Resources Research 44: W10422. https://doi.org/10.1029/2007WR006514

Lee, X., Goulden, M. L., Hollinger, D. Y., Barr, A., Black, T. A., Bohrer, G., … Zhao, L. (2011). Observed increase in local cooling effect of deforestation at higher latitudes. Nature, 479(7373), 384–387. https://doi.

org/10.1038/nature10588

Li, Y., Zhao, M., Mildrexler, D. J., Motesharrei, S., Mu, Q., Kalnay, E., …Wang, K. (2016). Potential and Actual impacts of deforestation and afforestation on land surface temperature. Journal of Geophysical Research: Atmospheres, 2016JD024969. https://doi.org/10.1002/2016JD024969

Li, Y., Zhao, M., Motesharrei, S., Mu, Q., Kalnay, E., & Li, S. (2015a). Local cooling and warming effects of forests based on satellite observations. Nature Communications, 6, 6603.

Li, Z. L., Tang, B. H., Wu, H., Ren, H., Yan, G., Wan, Z., … Sobrino, J. A. (2013). Satellite-derived land surface temperature: Current status and perspectives. Remote Sensing of Environment, 131, 14–37. https://doi.org/10.1016/j.rse.2012.12.008

Li, Z., Tang, H., Zhang, B., Yang, G., Xin, X. (2015b): Evaluation and Intercomparison of MODIS and GEOV1 Global Leaf Area Index Products over Four Sites in North China, Sensors, 15, 6196–6216, https://doi.org/10.3390/s150306196.

Lillesand, T.M., Kiefer, R.W., (1979) Remote Sensing and Image Interpretation, John Wiley and Sons, New York.

Lindroth, A., 1993. Aerodynamic and canopy resistance of short-rotation forest in relation to leaf area index and climate. Boundary-Layer Meteorol. 66, 265–279.

Liu, J., Schaaf, C., Strahler, A., Jiao, Z., Shuai, Y., Zhang, Q., … Dutton, E. G. (2009). Validation of Moderate Resolution Imaging Spectroradiometer (MODIS) albedo retrieval algorithm: Dependence of albedo on solar zenith angle, Journal of Geophysical Research, 114, 1–11. https://doi.org/10.1029/2008JD009969

Lobell, D. B., and G. P. Asner. (2002). Moisture effects on soil reflectance, Soil Sci. Soc. Am. J., 66, 722–727.

Loeb, N. G., Wielicki, B. A., Doelling, D. R., Smith, G. L., Keyes, D. F., Kato, S., ... Wong, T. (2009). Toward optimal closure of the Earth's top-of-atmosphere radiation budget, J. Clim., 22, 748–766, https://doi.org/10.1175/2008JCLI2637.1

Luyssaert, S. et al. (2014). Land management and land-cover change have impacts of similar magnitude on surface temperature. Nature Climate Change, 4, 389–393. https://doi.org/10.1038/NCLIMATE2196

Lyon, B., and Dewitt, D. G. (2012). A recent and abrupt decline in the East African long rains. Geophysical Research Letters, 39(2), 1–5. https://doi.org/10.1029/2011GL050337

Lyon, B. (2014). Seasonal drought in the Greater Horn of Africa and its recent increase during the March–May long rains. J. Clim. 27, 7953–7975. https://doi.org/10.1175/JCLI-D-13-00459.1.

Maeda, E. J., Wiberg, D., & Pellikka, P. K. E. (2011). Estimating reference evapotranspiration using remote sensing and empirical models in a region with limited ground data availability in Kenya. Applied Geography, 31, 251–258. https://doi.org/10.1016/j.apgeog.2010.05.011

Mahmood, R., Pielke, R. A., Hubbard, K. G., Niyogi, D., Dirmeyer, P. A., Mcalpine, C., … Fall, S. (2014). Land cover changes and their biogeophysical effects on climate. International Journal of Climatology, 34(4), 929–953. https://doi.org/10.1002/joc.3736

Martens, B., Miralles, D.G., Lievens, H., van der Schalie, R., de Jeu, R.A.M., Fernández-Prieto, D., Beck, H.E., Dorigo, W.A., and Verhoest, N.E.C. (2017). GLEAM v3: satellite-based land evaporation and root-zone soil moisture, Geosci. Model Dev., 10, 1903–1925.

Meng, X. H., Evans, J. P., and McCabe, M. F. (2014). The influence of inter-annually varying albedo on regional climate and drought, Clim. Dynam., 42, 787–803, doi:10.1007/s00382-013-1790-0.

Michael G. B, Santha A., Lawrence C.,

Richard C., Clara D., Ronald G.,… Max Suarez (2015). MERRA-2: Initial Evaluation of the Climate. Technical Report Series on Global Modeling and Data Assimilation Vol. 43.

Miralles, D.G., Gentine, P., Seneviratne, S.I., Teuling, A.J. (2018). Land-atmospheric feedbacks during droughts and heatwaves: state of the science and current challenges, Ann. N. Y. Acad. Sci., Special Issue: Climate Sciences. ISSN 0077-8923, https://doi.org/10.1111/nyas.13912

Miranda, H. S., Lloyd, J., Grace, J., Francey, R. J., Mcintyre, J. A., … Brass, J. b. (1997). Fluxes of carbon, water, and energy over Brazilian cerrado: An analysis using eddy covariance and stable isotopes. Plant, Cell Environ., 20(3), 315–328. https://doi.org/10.1046/j.1365-3040.1997.d01-80.x

Mohr K.I., Baker R.D., Tao, W. K., Famiglietti J. S. (2003). The sensitivity of West African convective line water budgets to land cover. Journal of Hydrometeorology 4: 62–76.

Moore, K.E., Fitzjarrald, D.R., Sakai, R.K. (1996). Seasonal variation in radiative and turbulent exchange at a deciduous forest in Central Massachusetts. Journal of Applied Meteorology, 35(1), 122-134. https://doi.org/10.1175/1520-0450(1996)035<0122

Myhre, G., D. Shindell, F.-M. Bréon, W. Collins, J. Fuglestvedt, J. Huang, D. Koch, J.-F. Lamarque, D. Lee, B. Mendoza, T. Nakajima, A. Robock, G. Stephens, T. Takemura and H. Zhang (2013). Anthropogenic and Natural Radiative Forc¬ing. In: Climate Change 2013: The Physical Science Basis. Contribution of Working Group I to the Fifth Assessment Report of the Intergovernmental Panel on Climate Change [Stocker, T.F., D. Qin, G.-K. Plattner, M. Tignor, S.K. Allen, J. Boschung, A. Nauels, Y. Xia, V. Bex and P.M. Midgley (eds.)]. Cambridge University Press, Cambridge, United Kingdom and New York, NY, USA

Myhre, G., Kvaleva, M. M., & Schaaf, C. B. (2005). Radiative forcing due to anthropogenic vegetation change based on MODIS surface albedo data. Geophysical Research Letters, 32, 2–5. https://doi.org/10.1029/2005GL024004

Naumann, G., Barbosa, P., Carrao, H., Singleton, A., & Vogt, J. (2012). Monitoring drought conditions and their uncertainties in Africa using TRMM data, J. Appl. Meteorol. Climatol., 51, 1867–1874, https://doi.org/10.1175/JAMC-D-12-0113.1

Nicholson, S. E. (1996). A review of climate dynamics and climate variability in Eastern Africa. In: The limnology, climatology and paleoclimatology of the East African lakes, CRC Press, pp 25–56

Nicholson, S. E., Some, B., McCollum, J., Nelkin E.,, D. Klotter, D., Berte, Y… Traore, A.K. (2003). Validation of TRMM and other rainfall estimates with a high-density gauge dataset for West Africa. Part II: Validation of TRMM rainfall products.

Nicholson, S. E. (2017). Climate and climatic variability of rainfall over eastern Africa. Reviews of Geophysics, 55(3), 590–635. https://doi.org/10.1002/2016RG000544

Notaro, M., Wang, F., & Yu, Y. (2019). Elucidating observed land surface feedbacks across sub-Saharan Africa. Climate Dynamics, 0(0), 0. https://doi.org/10.1007/s00382-019-04730-3

OECD/FAO (2016). Agriculture in Sub-Saharan Africa: Prospects and challenges. OECD-FAO Agricultural Outlook 2016-2025, 181(November 1947), 39. https://doi.org/10.1787/888933381341

Otterman, J. (1977). Anthropogenic impact on the albedo of the earth. Clim. Change 1977, 1 (2), 137−155.

Pellikka, P. K. E., Clark, B. J. F., Gosa, A. G., Himberg, N., Hurskainen, P., Maeda, E., … Siljander, M. (2013). Agricultural Expansion and Its Consequences in the Taita Hills, Kenya. Developments in Earth Surface Processes, 16(2006), 165–179. https://doi.

org/10.1016/B978-0-444-59559-1.00013-X
Penuelas, J., Rutishauser, T., & Filella, I. (2010). Phenology Feedbacks on. Science, 324(May 2009), 887–888.

Perugini, L. , Caporaso, L. , Marconi, S. , Cescatti, A., Quesada, B., De Noblet-Ducoudré, ... Arneth, A. (2017). Biophysical effects on temperature and precipitation due to land cover change. Environmental Research Letters, 12(5), https://doi.org/10.1088/1748-9326/aa6b3f

Pfeifer, M., Platts, P. J., Burgess, N. D., Swetnam, R. D., Willcock, S., Lewis, S. L., et al. (2012). Land use change and carbon fluxes in East Africa quantified using earth observation data and field measurements. Environmental Conservation, 40(3), 241–252. http://doi.org/10.1017/S0376892912000379

Pfeifroth, Uwe; Kothe, Steffen; Müller, Richard; Trentmann, Jörg; Hollmann, Rainer; Fuchs, Petra; Werscheck, Martin (2017): Surface Radiation Data Set - Heliosat (SARAH) - Edition 2, Satellite Application Facility on Climate Monitoring, https://doi.org/10.5676/EUM_SAF_CM/SARAH/V002 Pielke R. A, Marland G, Betts R. A., Chase T. N., Eastman J. L., Niles J. O., and

Mohr K.I., Baker R.D., Tao, W. K., Famiglietti J. S. (2003). The sensitivity of West African convective line water budgets to land cover. Journal of Hydrometeorology 4: 62–76.

Moore, K.E., Fitzjarrald, D.R., Sakai, R.K. (1996). Seasonal variation in radiative and turbulent exchange at a deciduous forest in Central Massachusetts. Journal of Applied Meteorology, 35(1), 122-134. https://doi.org/10.1175/1520-0450(1996)035<0122

Myhre, G., D. Shindell, F.-M. Bréon, W. Collins, J. Fuglestvedt, J. Huang, D. Koch, J.-F. Lamarque, D. Lee, B. Mendoza, T. Nakajima, A. Robock, G. Stephens, T. Takemura and H. Zhang (2013). Anthropogenic and Natural Radiative Forc¬ing. In: Climate Change 2013: The Physical Science Basis. Contribution of Working Group I to the Fifth Assessment Report of the Intergovernmental Panel on Climate Change [Stocker, T.F., D. Qin, G.-K. Plattner, M. Tignor, S.K. Allen, J. Boschung, A. Nauels, Y. Xia, V. Bex and P.M. Midgley (eds.)]. Cambridge University Press, Cambridge, United Kingdom and New York, NY, USA

Myhre, G., Kvaleva, M. M., & Schaaf, C. B. (2005). Radiative forcing due to anthropogenic vegetation change based on MODIS surface albedo data. Geophysical Research Letters, 32, 2–5. https://doi.org/10.1029/2005GL024004

Naumann, G., Barbosa, P., Carrao, H., Singleton, A., & Vogt, J. (2012). Monitoring drought conditions and their uncertainties in Africa using TRMM data, J. Appl. Meteorol. Climatol., 51, 1867–1874, https://doi.org/10.1175/JAMC-D-12-0113.1

Nicholson, S. E. (2017). Climate and climatic variability of rainfall over eastern Africa. Reviews of Geophysics, 55(3), 590–635. https://doi.org/10.1002/2016RG000544

Nicholson, S. E., Some, B., McCollum, J., Nelkin E.,, D. Klotter, D., Berte, Y… Traore, A.K. (2003). Validation of TRMM and other rainfall estimates with a high-density gauge dataset for West Africa. Part II: Validation of TRMM rainfall products.

Nicholson, S. E. (1996). A review of climate dynamics and climate variability in Eastern Africa. In: The limnology, climatology and paleoclimatology of the East African lakes, CRC Press, pp 25–56

Notaro, M., Wang, F., & Yu, Y. (2019). Elucidating observed land surface feedbacks across sub-Saharan Africa. Climate Dynamics, 0(0), 0. https://doi.org/10.1007/s00382-019-04730-3

OECD/FAO (2016). Agriculture in Sub-Saharan Africa: Prospects and challenges. OECD-FAO Agricultural Outlook 2016-2025, 181(November 1947), 39. https://doi.org/10.1787/888933381341

Otterman, J. (1977). Anthropogenic

impact on the albedo of the earth. Clim. Change 1977, 1 (2), 137−155.

Pellikka, P. K. E., Clark, B. J. F., Gosa, A. G., Himberg, N., Hurskainen, P., Maeda, E., … Siljander, M. (2013). Agricultural Expansion and Its Consequences in the Taita Hills, Kenya. Developments in Earth Surface Processes, 16(2006), 165–179. https://doi.org/10.1016/B978-0-444-59559-1.00013-X

Penuelas, J., Rutishauser, T., & Filella, I. (2010). Phenology Feedbacks on. Science, 324(May 2009), 887–888.

Perugini, L. , Caporaso, L. , Marconi, S. , Cescatti, A., Quesada, B., De Noblet-Ducoudré, ... Arneth, A. (2017). Biophysical effects on temperature and precipitation due to land cover change. Environmental Research Letters, 12(5), https://doi.org/10.1088/1748-9326/aa6b3f

Pfeifer, M., Platts, P. J., Burgess, N. D., Swetnam, R. D., Willcock, S., Lewis, S. L., et al. (2012). Land use change and carbon fluxes in East Africa quantified using earth observation data and field measurements. Environmental Conservation, 40(3), 241–252. http://doi.org/10.1017/S0376892912000379

Pfeifroth, Uwe; Kothe, Steffen; Müller, Richard; Trentmann, Jörg; Hollmann, Rainer; Fuchs, Petra; Werscheck, Martin (2017): Surface Radiation Data Set - Heliosat (SARAH) - Edition 2, Satellite Application Facility on Climate Monitoring, https://doi.org/10.5676/EUM_SAF_CM/SARAH/V002

Pielke R. A, Marland G, Betts R. A., Chase T. N., Eastman J. L., Niles J. O., and Running S. W. (2002). The influence of landuse change and landscape dynamics on the climate system: relevance to climate-change policy beyond the radiative effect of greenhouse gases Phil. Trans. R. Soc. A 360 1705–19

Pielke, R. A., Pitman, A., Niyogi, D., Mahmood, R., McAlpine, C., Hossain, F., … de Noblet, N. (2011). Land use/land cover changes and climate: Modeling analysis and observational evidence. Wiley Interdisciplinary Reviews: Climate Change, 2(6), 828–850. https://doi.org/10.1002/wcc.144

Pielke Sr, R. A. (2001). Influence of the spatial distribution of vegetation and soils on the prediction of cumulus convective rainfall. Reviews of Geophysics, 39(2), 151–177.

Pitman, A. J., Cruz, F. T., Davin, E. L., Bonan, G. B., Brovkin, V., Claussen, M., … Seneviratne, S. I. (2009). Uncertainties in climate responses to past land cover change: First results from the LUCID intercomparison study. Geophys. Res.Lett. 36, 1–6. https://doi.org/10.1029/2009GL039076

Ramankutty, N. and Foley J., A. (1999). Estimating historical changes in global land cover: croplands from 1700 to 1992. Global Biogeochemical Cycles 13: 997–1027. DOI: 10.1029/1999GB900046

Raupach, M.R., (1994). Simplified expressions for vegetation roughness length and zero-plane displacement as functions of canopy height and area index. Boundary-Layer Meteorol. 71, 211–216.

Richardson, A. D., Keenan, T. F., Migliavacca, M., Ryu, Y., Sonnentag, O., & Toomey, M. (2013). Climate change, phenology, and phenological control of vegetation feedbacks to the climate system. Agricultural and Forest Meteorology, 169, 156–173. https://doi.org/10.1016/j.agrformet.2012.09.012

Rigden, A. J., & Li, D. (2017). Attribution of surface temperature anomalies induced by land use and land cover changes. Geophysical Research Letters, 44(13), 6814–6822. https://doi.org/10.1002/2017GL073811

Rowell, D.P., Booth, B.B.B., Nicholson, S.E., Good, P. (2015). Reconciling past and future rainfall trends over East Africa. J. Clim. 28, 9768–9788. https://doi.org/10.1175/JCLI-D-15-0140.1.

Running, S., Mu, Q., Zhao, M. (2017). MOD16A2 MODIS/Terra Net

Evapotranspiration 8-Day L4 Global 500m SIN Grid V006. NASA EOSDIS Land Processes DAAC. https://doi.org/10.5067/MODIS/MOD16A2.006

Ryu, Y., Baldocchi, D.D., Ma, S., Hehn, T. (2008). Interannual variability of evapotranspiration and energy exchange over an annual grassland in California. Journal of Geophysical Research: Atmospheres. 113(D9).

Samain, O., Kergoat, L., Hiernaux, P., Guichard, F., Mougin, E., Timouk, F., & Lavenu, F. (2008). Analysis of the in situ and MODIS albedo variability at multiple timescales in the sahel. Journal of Geophysical Research Atmospheres, 113(14), 1–16. https://doi.org/10.1029/2007JD009174

Schaaf, C. B., Gao, F., Strahler, A. H., Lucht, W., Li, X., Tsang, T., … Roy, D. (2002). First operational BRDF albedo nadir reflectance products from MODIS. Remote Sensing of Environment, 83(1-2), 135-148. https://doi.org/10.1016/S0034-4257(02)00091-3

Schmugge, T. J. and Becker, F. (1991). Remote Sensing Observations for the Monitoring of Land-Surface Fluxes and Water Budgets. In: Schmugge T.J., André JC. (eds) Land Surface Evaporation. Springer, New York, NY. https://doi.org/10.1007/978-1-4612-3032-8_20

Seneviratne, S. I., Lüthi D., Litchi M., Schär C. (2006). Land–atmosphere coupling and climate change in Europe. Nature 443, 205–209. https://doi.org/10.1038/nature05095

Seneviratne, S. I., Phipps, S. J., Pitman, A. J., Hirsch, A. L., Davin, E. L., Donat, M. G., … Kravitz, B. (2018). Land radiative management as contributor to regional-scale climate adaptation and mitigation. Nature Geoscience, 11(2), 88–96. https://doi.org/10.1038/s41561-017-0057-5

Shaw, R.H., Pereira, A.R., (1982). Aerodynamic roughness of a plant canopy: a numerical experiment. Agric. Meteorol. 26, 51–65.

Song, J. (1999). Phenological influences on the albedo of prairie grassland and crop fields. International Journal of Biometeorology, 42(3), 153-157. https://doi.org/10.1007/s004840050099

Sütterlin, M., Stöckli, R., Schaaf, C. B, Wunderle, S. (2016). Albedo climatology for European land surfaces retrieved from AVHRR data (1990–2014) and its spatial and temporal analysis from green-up to vegetation senescence, J. Geophys. Res.-Atmos., 121, 8156–8171, https://doi.org/10.1002/2016JD024933

Teillet, P.M., Guindon, B., Goodenough, D.G. (1982). On the slope-aspect correction of multispectral scanner data. Can. J. Remote Sens. 8 (2), 84–106. https://doi.org/10.1080/07038992.1982.10855028

Teuling, A. J., Seneviratne, S. I., Stöckli, R., Reichstein, M., Moors, E., Ciais, P., … Klumpp, K. (2010). Contrasting response of European forest and grassland energy exchange to heatwaves, Nat. Geosci., 3(10), 722–727, https://doi.org/10.1038/ngeo950

Teuling, A. J., and Seneviratne, S. I. (2008). Contrasting spectral changes limit albedo impact on land-atmosphere coupling during the 2003 European heat wave, Geophys. Res. Lett., 35, L03401, https://doi.org/10.1029/2007GL032778.

Trezza, R., Allen, R. G., & Tasumi, M. (2013). Estimation of actual evapotranspiration along the Middle Rio Grande of New Mexico using MODIS and Landsat imagery with the METRIC model. Remote Sensing, 5(10), 5397–5423. https://doi.org/10.3390/rs5105397

Uhe, P., Philip, S., Kew, S., Shah, K., Kimutai, J., Mwangi, E., … Otto, F. (2018). Attributing drivers of the 2016 Kenyan drought. International Journal of Climatology, 38(December 2017), e554–e568. https://doi.org/10.1002/joc.5389

UN DESA (2019). World Population

Prospects: The 2019 Revisions, New York.
UNOCHA (2011). Eastern Africa drought humanitarian report. UN Office for the Coordination of Humanitarian Affairs Rep, vol 4

Verger, A., Camacho, F., Goten, R.V., Jacobs, T. (2014). Product user manual, Leaf area index (LAI), fraction of absorbed photosynthetically active radiation (FAPAR), fraction of vegetation cover (FCover), collection 1 km, version 2. Issue 1.32. Copernicus.

Wan, Z., Zhang, Y., Zhang, Q., & Li, Z. (2002). Validation of the land surface temperature products retrieved from Terra Moderate Resolution Imaging Spectroradiometer data. Remote Sensing of Environment, 83(1), 163-180. https://doi.org/10.1016/S0034-4257(02)00093-7

White, F. (1983). The vegetation of Africa: a descriptive memoir to accompany the UNESCO/AETFAT/UNSO vegetation map of Africa. Natural Resources Research (Vol. 20). https://doi.org/10.2307/2260340

WMO (World Meteorological Organization) (2012). Standardized Precipitation Index User Guide (M. Svoboda, M. Hayes and D. Wood), WMO-No. 1090, Geneva.

Yang, W., Tan, B., Huang, D., Rautiainen, M., Shabanov, N. V, Wang, Y., … Myneni, R. B. (2006). MODIS Leaf Area Index Products: From Validation to Algorithm Improvement, IEEE Transactions on Geoscience and Remote Sensing, 44(7), 1885–1898. https://doi.org/10.1109/TGRS.2006.871215

Yin, D., Roderick, M. L., Leech, G., Sun, F., and Y. Huang, Y. (2014). The contribution of reduction in evaporative cooling to higher surface air temperatures during drought, Geophys.Res.Lett.,41,7891–7897, doi:10.1002/2014GL062039.

Zhang, X., Friedl, M. A., Schaaf, C. B., Strahler, A. H., & Liu, Z. (2005). Monitoring the response of vegetation phenology to precipitation in Africa by coupling MODIS and TRMM instruments. Journal of Geophysical Research D: Atmospheres, 110(12), 1–14. https://doi.org/10.1029/2004JD005263